Incorporating High-Impedance-Fault Detection Functionality in Distribution System Online Monitoring: An Alternative to Existing Methods

by

Adel Tabakhpour Langeroudi

A THESIS SUBMITTED IN PARTIAL FULFILLMENT OF

THE REQUIREMENTS FOR THE DEGREE OF

MASTER OF APPLIED SCIENCE

in

THE COLLEGE OF GRADUATE STUDIES

(Electrical Engineering)

THE UNIVERSITY OF BRITISH COLUMBIA

(Okanagan)

January 2021

The following individuals certify that they have read, and recommend to the College of Graduate Studies for acceptance, a thesis/dissertation entitled:

Incorporating High-Impedance-Fault Detection Functionality in Distribution System Online Monitoring: An Alternative to Existing Methods

submitted by	Adel Tabakhpour Langeroudi	in partial fulfillment of the requirements for
the degree of	Master of Applied Science	
in	Electrical Engineering	

Examining Committee:

Dr. Morad Abdelaziz, Faculty of Applied Science, UBC Okanagan

Supervisor

Dr. Liwei Wang, Faculty of Applied Science, UBC Okanagan

Supervisory Committee Member

Dr. Christine Chen, Electrical and Computer Engineering, UBC Vancouver

Supervisory Committee Member

Dr. Sina Kheirkhah, Faculty of Applied Science, UBC Okanagan

University Examiner

Abstract

The increasing deployment of informatics and communication systems in distribution systems (DS)s enables many desirable functionalities such as optimal control of distributed energy resources, online fault detection, online topology identification and energy theft detection. In this thesis, we focus on exploiting this emerging monitoring and control infrastructure to address high-impedance faults (HIF)s. HIFs have long been recognized as a serious protection issue in DSs, which can adversely impact the DS safety and protection as well as its operation and profitability. Trees contacting overhead lines and deteriorated insulators (due to cracks, dust, humidity, ice, etc.) are the main triggers of HIF in DSs. Once created, HIF imposes a large impedance between two phases or to the ground (through a third object like a tree or the utility poles). Given its high impedance value, HIF usually draws a relatively small current, less than the nominal load level, making it undetectable for relay protection systems. However, the persistent existence of HIF dissipates significant electric power on the long-term, which is undesirable for DS profitability and operation. More importantly, the existence of such HIFs presents weak points in the DS that can easily deteriorate to arcing faults, raising major safety concerns. Existing literature on HIF detection exploit the nonlinear and transient properties of the HIF current, which depends on the use of measurements with high sampling rates (several kHz to MHz) to enable the extraction of the features corresponding to the HIF by applying appropriate signal processing techniques. As such, these approaches demand high-resolution measurements, which are not necessarily economical or available for many distribution systems. On the other hand, today's distribution systems are mostly equipped with other types of measurements that are far slower than those required by the existing HIF detection algorithms. These measurements are however transmitted

to one central unit and are typically processed together for DS static state estimation. This thesis proposes to take advantage of this and to enable the detection of HIFs using the static DS state estimation. The HIF detection problem is accordingly re-defined in a static framework and the HIF is modeled as a parameter to be estimated from the measurements available to the central state estimator from different sources including SCADA, smart meters and PMU measurements. The distribution system state estimation model is augmented to allow for the proposed HIF detection functionality. The IEEE 13-bus and 123-bus systems are used to evaluate the effectiveness of the proposed approach.

Lay Summary

High-impedance faults (HIF)s are faults that draw current so small for detection by the protection system. The negative effects of HIFs include loss of power and profitability, insulation and cable aging, more frequent maintenance requirements and safety concerns. Existing literature on HIFs detection propose using measurements with very high sampling rates (of up to MHz) to extract the nonlinear and transient features that correspond to the HIF. However, equipping every single line of the distribution system with such measurements and their corresponding data communication and processing systems is far from economical for today's distribution systems. On the other hand, many of today's distribution systems are already equipped with slow-rate measurements of rates varying from $5 \times 10^{-4} Hz$ (SCADA measurements) up to $60\ Hz$ (PMU measurements), which are serving already in many valuable functionalities such as load prediction, distributed energy resources' optimal control, system topology identification, system states and parameter monitoring, energy theft detection, etc. We propose using the existing measurement infrastructure for detection and location of the HIF, by processing the measurements from all over the system simultaneously at the central monitoring unit. The framework of the HIF location problem is formulated for this purpose and an algorithm is proposed that detects and locates the HIF in distribution systems.

Preface

This work is based on the research performed at the School of Engineering at the University of British Columbia (Okanagan Campus) by Adel Tabakhpour Langeroudi, under the supervision of Dr. Morad Abdelaziz. The results from this research are published in the following articles:

- A. Tabakhpour L., and M. M. A. Abdelaziz, "Preventative high impedance fault detection using distribution system state estimation." Electric Power Systems Research 186 (2020): 106394.
- A. Tabakhpour L., and M. M. A. Abdelaziz, "Neural Network Model for False Data Detection in Power System State Estimation," 2019 IEEE Canadian Conference of Electrical and Computer Engineering (CCECE), Edmonton, AB, Canada, 2019, pp. 1-5.
- A. Tabakhpour L. and M. M. A. Abdelaziz, "Enhanced Bad Data Identification in Distribution System State Estimation," 2018 IEEE Canadian Conference on Electrical & Computer Engineering (CCECE), Quebec City, QC, 2018, pp. 1-5.

Table of Contents

Abstract ..... **iii**

Lay Summary ..... **v**

Preface ..... **vi**

Table of Contents ..... **vii**

List of Tables ..... **x**

List of Figures ..... **xi**

List of Symbols ..... **xii**

List of Abbreviations ..... **xiii**

Acknowledgements ..... **xiv**

Dedication ..... **xv**

Chapter 1: Introduction **1**

1.1 High-impedance faults in distribution systems 1

1.1.1 High impedance fault origins 3

1.1.2 Existing high impedance fault detection methods 3

1.2 Proposed approach to HIF detection 6

1.2.1 Existing distribution system online measurement schemes 8

1.2.2 Distribution system state estimation 10

1.2.2.1 State selection in distribution system state estimation 11

1.2.2.2 State estimation algorithms 13

1.2.3 Proposed HIF detection based on existing online measurement schemes 16

Chapter 2: Distribution system model and state estimation **19**

2.1 Overview 19
2.2 Distribution system mathematical model 20
2.3 Integrating high-impedance fault in static model of distribution system 24
2.3.1 Transformation between actual T-model and equivalent π-model 25
2.3.2 Power loss calculation at the HIF location 28
2.4 Distribution system state estimation 30
2.4.1 Modeling HIF in distribution system state estimation with constant admittance 31
2.4.2 Modeling HIF in distribution system state estimation with constant power 34
2.5 Summary 37
Chapter 3: HIF location procedure and considerations 39
3.1 Overview 39
3.2 Detection of HIF existence in the system 39
3.3 Without intrinsic error correction (Plan A) 43
3.4 With intrinsic error correction (Plan B) 44
3.5 Observability and Measurement Placement 46
3.6 Summary 47
Chapter 4: Simulation results 49
4.1 Overview 49
4.2 Measurement placement 50
4.3 Detection of HIF existence 51
4.4 HIF line identification 53
4.5 HIF distance estimation from the nodes 57
4.6 Individual HIF simulation 58

4.7 Determining the HIF location performance on different nodes of the system 60

4.8 Computational specification of the state estimation 63

4.9 Summary 64

Chapter 5: Conclusion 65

5.1 Summary 65

5.2 Future work 66

Bibliography 67

List of Tables

Table 2.1 Distribution system mathematical model definitions used in this thesis 22

Table 2.2 Notation of variables and parameters 22

Table 4.1 Measurement placement results for the 13-node feeder 51

Table 4.2 Measurement placement results for the 123-node feeder 51

Table 4.3 HIF existence detection performance in 13-node and 123-node feeders..... 52

Table 4.4 HIF line identification in 13-node feeder in different conditions 55

Table 4.5 HIF line identification in 123-node feeder in different conditions 56

Table 4.6 Individual HIF line identification results: HIF on line 632-633 phase *a* 58

Table 4.7 Individual HIF line identification results: HIF on line 671-675 phase *b* 59

Table 4.8 Individual HIF line identification results: HIF on line 671-680 phase *b* 59

Table 4.9 Individual HIF line identification results: HIF on line 632-633 phase *c* 59

Table 4.10 Individual HIF line identification results: HIF on line 632-645 phase *c* 59

Table 4.11 Individual HIF line identification results: HIF on line 632-671 phase *c* 60

Table 4.12 Computational specification of the proposed HIF estimation method 63

List of Figures

Figure 1.1 HIF origins 2

Figure 1.2 Overhead wire breakdown and contact to ground 3

Figure 1.3 A distribution system monitored by SCADA, PMU and Smart meters 9

Figure 1.4 Research on distribution system state estimation 13

Figure 1.5 Existing and proposed HIF detection schemes 16

Figure 2.1 HIF static model in distribution system 25

Figure 3.1 HIF detection flowchart 44

Figure 4.1 HIF distance estimation error in lines 58

Figure 4.2 The steps of changing the HIF 61

Figure 4.3 Performance criteria (4.2) for HIF line identification in 13-node feeder 62

Figure 4.4 Performance criteria (4.2) for HIF line identification in 123-node feeder 62

List of Symbols

Notation	Definition
V_i^{abc}, δ_i^{abc}	Three-phase voltage magnitude and angle of node *i*
P_i^{abc}, Q_i^{abc}	Three-phase active and reactive injected power of node *i*
P_{ij}^{abc}, Q_{ij}^{abc}	Three-phase active and reactive flow power at branch *i-j*
I_{ij}^{abc}, α_{ij}^{abc}	Three-phase current magnitude and angle at branch *i-j*
$\tilde{Z}_{ij}^{abc}$	Three-phase impedance matrix of branch *i-j*
$\tilde{Y}_{ii}^{abc}$	Three-phase admittance of node *i*
$\tilde{Y}_{ij}^{abc}$	Three-phase mutual admittance between node *i* and *j*
z	Measurement vector
x	States vector
$h(.)$	Observation function
ω	Measurement noise

List of Abbreviations

CT	Current transformer
DS	Distribution system
HIF	High-impedance fault
PMU	Phasor measurement units
PT	Potential transformer
RMS	Root mean square
SCADA	Supervisory control and data acquisition
SE	State estimation
WLAV	Weighted least absolute value
WLS	Weighted least squares
WAMS	Wide-area monitoring system

Acknowledgements

I offer my enduring gratitude to the faculty, staff and my fellow students at UBC, University of Guilan and Iran University of Science and Technology, who have inspired me to continue my work in this field.

I thank Dr. Alfred Baghramian for supporting me to continue my studies abroad, and Dr. Siamak Farshad for giving me the real engineering and mathematical thinking in the actual world, and showing the way by being the exemplary engineer, technically and ethically.

Special thanks are owed to my wife, Samira.

And special thanks to my parents, Souri and Ebrahim.

Dedication

This thesis is dedicated to Professor Morad Abdelaziz for his limitless understanding and priceless support.

Chapter 1: Introduction

High-impedance faults have a unique position in the research history in the area of distribution systems for two reasons. First, HIF currents are in the operational range of the distribution system currents, which requires specific methods for its detection and treatment distinct from the over-current relays. Second, the HIF is not as destructive to distribution systems as the short-circuit faults, and many distribution systems have high-impedance faults in their operational conditions. Therefore, the operators tend to neglect the HIF if it does not impose any safety problem or damage to the human or environment. The research in this area is accordingly not mature enough to be applied to all distribution systems due to the significant cost of the proposed methods in the literature.

In the first chapter, we specify the advancement of the existing research on the HIF in distribution systems and evaluate the possibility of applying these methods in the actual distribution systems. Then we introduce the proposed method in this thesis for HIF detection and location, which is based on the modern online monitoring of the distribution system that uses the state estimation. To do so, the existing literature on the distribution system state estimation and its online monitoring is reviewed briefly, which will be used to develop the proposed method.

1.1 High-impedance faults in distribution systems

Distribution system is quite exposed to the environment due to its nature. It is inevitable to prevent the system from the frequent faults and flaws. For example, the objects contacting the pole-mounted wires in the rainy days can cause short-circuit faults. The pole-mounted cables are more resilient to such faults, yet lightning strikes can, for instance, result in instantaneous

overvoltage and considerable currents passing through the cables, in addition to the vulnerability of their connection points to different types of faults. The underground distribution lines are safer compared with the pole-mounted networks, however, they suffer from the higher maintenance costs in case of faults, due to harder access to the underground cables by digging the earth. Thus, the distribution systems are designed to reduce the negative impacts of such faults and interruptions. For example, the relay protection system is always a very important part of the system design, which detects and removes the faults immediately by de-energizing the faulted feeder. However, the high-impedance faults (HIF) possess a special position in the distribution systems faults due to its special characteristic, that is, it draws the currents in the operational range of the system [1], which remains undetectable for the relay protection systems.

(a) A slum in Brazil

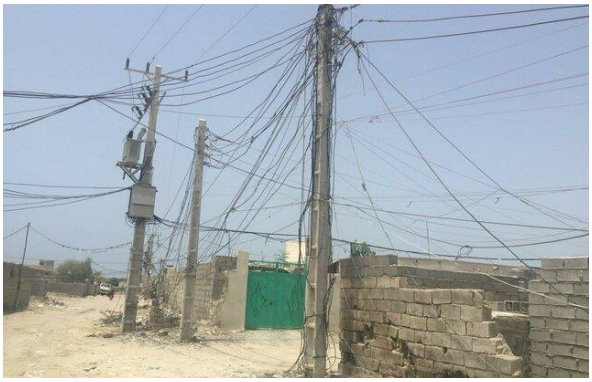

(b) Sistan, Iran

(c) San Francisco, USA

(d) Allahabad, India

Figure 1.1 HIF origins; images are taken from (a) Documentary movie "Pandora's Promise" by Robert stone, 2013, (b) ISNA, Iranian Students' News Agency, (c) https://www.govtech.com/ and (d) https://www.wsj.com/

1.1.1 High impedance fault origins

Contact of the pole-mounted wires to the trees, the deterioration of the insulators as a result of aging, surface dust or humidity, birds' dead body, etc., are among the primal causes of the HIF, which are quite common in distribution systems. Some other causes of HIF in distribution systems in the rural areas are the human activities. For example, using the utility poles to support small structures or for hanging the clothes, unsafe design of the feeders close to the homes' walls, over-extending the existing feeders to many customers, electricity theft, etc., are among other causes of HIF. Figure 1.1 shows several common origins of high-impedance fault in distribution systems.

In addition, a different type of HIF happens when one or some of the overhead wires break and falls on the ground. In this case, if the ground is dry enough to impose a high-impedance between the phase and the electrical ground, then the fault current will be in the operational range of the load currents, which is classified as HIF. Figure 1.2 shows examples of such high-impedance fault, which is usually accompanied by arcs as can be seen.

(a) (b)

Figure 1.2 Overhead wire breakdown and contact to ground (a) from [1] **and (b)** [2]

1.1.2 Existing high impedance fault detection methods

The impedance of HIF, as considered in the literature, varies from 400 Ω [3] to 15 kΩ [4]–[6] depending on its origins, which is in the range of normal loads operating in the distribution

systems. Therefore, the current magnitude of the HIF cannot be used alone to detect the HIF. However, the HIF connection point is usually unstable, as can be seen in figures 1.1 and 1.2, and its current contains a high harmonic contents. Traditionally in the literature, the frequency-domain characteristics of the current or power of HIF is used for its detection. Thus, the HIF detection problem is traditionally defined as a feature extraction problem from the HIF current or power waveform. For example in [5], [6], it is concluded from simulation results that specific frequencies are corresponding to the HIF, which are in the range of the MHz. In order to enable extraction of MHz frequencies from the HIF current waveform, the current should be measured at least by sampling rate more than twice the desired frequencies according to Nyquist's sampling theorem. However, equipping all the feeders with such high sampling rate measurements is infeasible in today's distribution systems. Therefore, the HIF remained a substantial problem, which is unsolved as of today. On the one hand, there are many HIF in different points of many operating distribution systems that are undetected [1], and are causing trouble for the optimal operation of the system. On the other hand, due to its high-impedance, HIF does not usually impose immediate safety or security issues, that pushes the operators to forget about investing on the very high-cost measurements with high-sampling rates. As a result, HIF remained a problem that exists in distribution system for a long time, while there is no economically feasible solution in the actual systems. In theory, the feature extraction approach can successfully detect the HIF, however, this approach is far beyond the economical limits of today's distribution systems.

HIF usually progresses over time to draw a small current, which is highly non-stationary and non-predictable [2]. The transient and nonlinear properties of HIF are mainly used in the literature for its detection by different signal analysis and feature extraction techniques. A constant HIF without any associated arcs or disturbances is hardly investigated as an issue, despite the long-

term aggregate power loss and safety concerns of such HIFs. In [7] and [8] a combination of anti-parallel diodes with a variable resistance is considered as the HIF model and different signal processing techniques are used to extract specific HIF features from high-resolution current measurements. A wavelet transform, independent of system model, is used for HIF detection in [9]. A pattern classifier, whose inputs are the waveform energy in addition to the time-frequency moments, is proposed for HIF detection in [10]. The works in [11]-[12] attempted to detect HIFs by analyzing the harmonic content of the current measurements and detecting the harmonic signature typically associated with frequent arcs appearing in case of tree contact or insulator breakdown. The harmonic contents of the high-resolution current measurements are considered as states in [13] and the problem of HIF detection is formulated for Kalman filter, with magnitude of different harmonic content of the HIF current waveform as observations. Feature extraction is detailed and a systematic approach is taken for feature selection in [3]. An elaborate feature selection is also proposed in [14] for the same purpose. The magnetic-field measured around overhead lines is used in [15] to detect HIFs existence. Transferring wave equations in power lines are solved for the maximum likelihood of fault location with time-reversal theory in [16]. Considering a single line with high-resolution measurements at one end, the problem of HIF is formulated for estimation in [17], where measured waveforms are sampled at high sampling rates and the HIF distance from the end node is estimated. In addition, some field experiments have been conducted on different HIFs at Texas A&M University, based on which a practical device was built to locate HIFs [2].

The works surveyed so far assumed the availability of high-resolution measurement devices over the line where the HIF happens. In contrast with these methods, the detection schemes in the [4]–[6], [18], [19] are designed for HIF detection in an entire distribution system rather than

in a single line. A measurement architecture is proposed based on power line modems in [18], which are able to deliver a sampling rate in the MHz range, and a classification method is used to detect HIF. A wide-area estimation approach is taken in [19] based on normalized residuals for general fault location. DS model-based approaches attempted the evaluation of line impedances in presence of HIF, as in the approach presented in [5], [6] and later extended to multi-conductor network in [4]. This approach is based on an impulse signal injection to the system and analyzing the impulse response on certain frequencies which are shown to carry information about the HIF location. This approach is designed for medium voltage systems, whose end transformer is delta-connected and acts as open-circuit for the studied frequencies. Even though it is a strong approach for HIF detection, it cannot be applied for the low-voltage where the transformer is star-connected with neutral connection. On the other hand, HIFs are still likely to happen in low-voltage networks due to less maintenance and lower height of overhead lines, especially in lines far from the main feeders or in rural areas. Reference [20] addresses the problem of multiple location estimation of HIF in DS model-based approaches. In addition, use of even harmonics is suggested for HIF detection in [21], where also it is proposed to modify all of the smart meters to report even harmonics of the node they are measuring. In this way, they could enable HIF detection over the entire DS, however, equipping all of smart meters with several even harmonic measurements pose significant cost to the monitoring system, considering all communication and computation needs.

1.2 Proposed approach to HIF detection

As explained, the existing HIF detection methods require measurements of the current waveforms at a very high sampling rate, which is not in the feasible economical limits of today's distribution systems. On the other hand, modern distribution systems are moving toward the online

measurement schemes with much lower sampling rates from 1 sample per 30 minutes in old SCADA measurements up to 60 samples per seconds in modern PMU measurements. These modern measurement infrastructure provide various desirable functionalities for distribution systems, such as optimal control of distributed generation units, system model and parameter estimation and correction, load prediction, fault location, energy theft detection, etc. We propose a state-estimation approach that uses the existing online measurement schemes for HIF detection and location.

The existing HIF detection methods [1]-[21] are mainly concerned with HIFs from a protection standpoint and attempt to detect those HIFs that cause safety issues due to arcs or other disturbances, by extracting the transient and nonlinear properties of HIF from high-resolution measured waveforms. Persistent high-impedances in the system, which have not yet progressed to arcing are however less focused on. Such high-impedances can develop in DSs in different ways, important among which are those due to leakage impedances. For example, [22]–[24] investigate the leakage impedance of insulators polluted with salty sea water, intense fog, and different surface pollutants, respectively. The leakage current on silicone rubber insulators under thermal and electrical stress is investigated in [25]. Such leakage impedances may result in flashover on the long-term if not resolved. The probability of flashover as a result of polluted insulators is studied in [26]. Although the leakage impedance may not cause immediate safety and flashover problems, their power loss will be considerable on the long-term, and their detection will prevent their future hazardous impacts. Thus, in many DSs periodical tests of insulators are routinely performed. Yet the surveyed papers and other research on the subject in the literature have not properly addressed the need for detecting these types of persistent HIFs before they develop into arcing faults. We propose the detection of such HIFs using DS state estimation (SE). As such, in this work the

problem is defined in a static framework and the HIF is modeled as a parameter to be estimated from the phasor measurements available in the system from different sources such as SCADA, smart meters, PMU measurements, etc.

1.2.1 Existing distribution system online measurement schemes

With the increasing penetration of the renewable energy resources in the modern distribution systems (DS), the online monitoring and control has become of vital importance for optimal, secure, safe and uninterrupted operation of the DS. There are different strategies depending on the operators' approach to the system operation. For example in the smart grid approach, the consumer side is equipped with the smart meters [27], which provide bi-directional communication paths to i) transfer the measurement data from the consumer side to the monitoring center and ii) provide the consumers with the online pricing to involve them in the optimal operation of the system. SCADA systems are also widely used in the distribution systems, which enables online measurement of the system in with a slow sampling rate pertaining to the slow dynamics of the traditional distribution systems [28]. In the modern distribution systems, PMU provide online measurement of the system at a far faster sampling rate [29] , where the dynamics are more critical due to the integration of distributed generation units. The sampling rate varies for SCADA systems between one sample per second up to one sample per several minutes, whereas that of PMU varies between 60 Hz down to 20 Hz in different references.

In general, an online measurement system for distribution system involves three main parts:

- Measurement equipment: potential transformers (PT), current transformers (CT), the analog/digital converters, noise filters, etc.
- Communication routes: wireless senders and receivers, optical fibres, communication cables, etc.

- Data processing equipment: the processors that receive the measurement data, process, filter and encrypt them and send them to the according points of the control and monitoring system

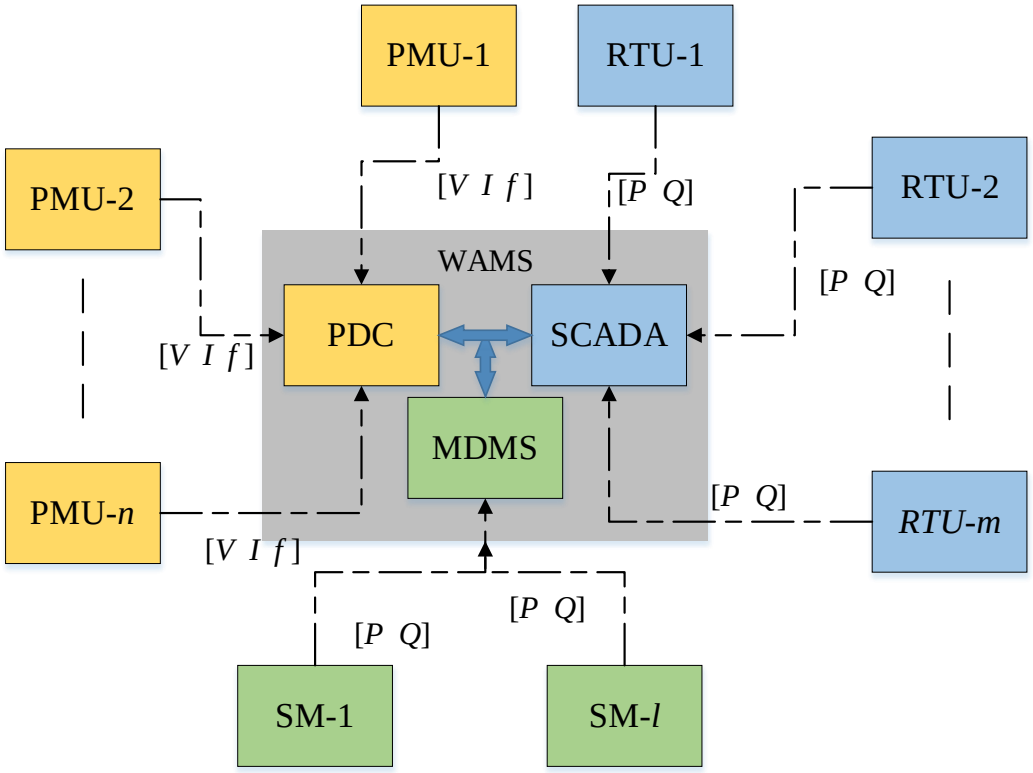

Figure 1.3 A distribution system can be monitored by SCADA, PMU and Smart meters simultaneously
PMU: Phasor measurement units; PDC: phasor data concentrators;
SM: Smart meters; MDMS: Meter data management system
RTU: Remote terminal unit; SCADA: Supervisory control and data acquisition

The three online measurement approaches, namely, smart meters, SCADA systems and PMUs, differ from each other in terms of all three aspects of measurement devices used to measure the electrical (and rarely mechanical) quantities, communication protocols used to transfer the measured data, and the data gathering and processing strategies. After all, from operators' standpoint, the major difference between them can be summed up as follows:

- Smart meter: provides bi-directional communication to involve the consumers in the optimal operation of distribution system by informing them of system condition and price. The sampling rate varies in different references.
- SCADA: provides unidirectional communication similar to PMU, with slow sampling rate from a sample per 30 minutes to a sample per 1 second. Suitable for traditional distribution systems where the dynamics are slow.
- PMU: provides fast sampling rate, from 20 Hz up to 60 Hz. Suitable for active distribution system with several distributed generation units that involve fast dynamics and require stability monitoring and control functions. PMUs are thus more expensive to implement compared with SCADA systems.

1.2.2 Distribution system state estimation: literature review, challenges and discussion

Even the most accurate measurement in any system contains an error compared with the true value it is measuring. The error has several different sources depending on the system and measurement infrastructure. In distribution system, the measurement errors may come from the measurement devices' noise or bias (due to aging for instance), occurring in the data transmission due to communication interference, as a result of digitalizing/compressing the numerical values, etc. Generally, the errors can be categorized in two classes of noise and bias. The former is the zero-mean and usually small error, which is inevitable; whereas the latter, bias, is the systematic error of the measurement infrastructure that should be avoided. To translate the noisy and erroneous measurement into the most likely system state estimate, is the main task of state estimation, in addition to the other functionalities that are discussed in what follows. The state estimation uses the mathematical system model (i.e. power flow equations derived from KVL and KCL laws) along with the measurements to estimate the system states. The most important aspects

of distribution system state estimation, which have become the focus of many researches, are discussed in the following along with the corresponding references. The reason of the state estimator selected in this thesis is also explained next to the corresponding references, by providing cons and pros analysis. The study of power system state estimation was developed as a discrete topic in late 1960s, and has been an active and dynamic research area ever since. The amount of relevant references are enormous in this area, thus only the most important references that pinpoint the ongoing research directions in the state estimation area are surveyed in this section, in addition to those references that leads to the development of the proposed HIF detection method based on distribution system state estimation in the current thesis.

1.2.2.1 State selection in distribution system state estimation

The selection of system states is one important aspect of the state estimation. A distribution system can be represented by different selection of variables as states. In the literature, two major selection of states are advocated, which are node voltage phasors [30] and branch current phasors [31]. In one special case, the powers are considered as states [32]. The phasor representation of the variables will be discussed in chapter 2. All of the estimators considered in the literature work with the real values, thus the phasors are themselves represented by separate polar or Cartesian representation. For example, angle and magnitude of node voltages or branch currents can be selected as states, which are real value representation of complex values (polar form). Real and imaginary parts of the node voltages or branch current can be also used as the states (Cartesian form). Each selection of states has cons and pros compared with others, which are the focus of many researchers in this area. The state selection of many references are listed and compared in [27]. Historically, Schweppe was the first to formulate the power system equations for estimation in 1970 [30], who considered the node voltages in polar form (i.e. the voltage magnitudes and

voltage angles of all nodes, resulting in number of states equal to number of nodes times two). Schweppe's model was proposed for the single-phase representation of the symmetrical power systems, which could be easily extended to the unbalanced three-phase systems. In 1994, Baran proposed use of branch-current for three-phase state estimation of distribution systems [31], where the main motivation was to increase the sparsity of the measurement matrix. The most significant step in the computations of the conventional state estimators is the inversion of the measurement matrix (that is the gradient/Jacobian of the measurement function). The branch-current-based state estimators' measurement matrix is sparser compared with the node-voltage-base estimators, thus its computations could be possibly lighter. However, the branch-current-based algorithms require the transformation of branch currents to the node voltages at the end of each estimation iteration to obtain the other system's dependent variables, and then transformation of the voltages back to the currents at the start of each estimation iteration in order to form the branch-current-based estimation. The voltage-current transformation might require much less computations compared with the matrix inversion depending on the system size and observability. Therefore, the branch-current-based algorithm can have actually less computations compared with the node-voltage-based estimators. However, one major disadvantage of the branch-current-based estimators is the complexity of the algorithm itself. In order to solve the system one time based on the system currents and then one time based on the system voltages, the topology matrices have to be saved and accessed actively in different forms. For example, when the distribution system is updated by adding one feeder, it is much harder to update the branch-current-based estimator algorithm. Whereas the node-voltage-based estimator only requires the admittance matrix for power flow equations, and which uses the topology in terms of from-to vectors of bus numbers. Thus only one matrix is required in the node-voltage-based estimator to represent the topology, whereas in the

branch-current-based estimator three different topology matrices are required that are the system branch-current incident matrix for the estimator, the system from-to topology matrix for power flow equations, and the system branch-node incident matrix for the voltage-current transformation. In a sufficiently small system, the branch-current-based estimator is certainly more complex and more time-consuming than the node-voltage-based estimator, because the time of back and forth transformation between currents and voltages are not compensated sufficiently by the improvement of matrix inversion due to more sparsity (in small systems). Therefore, for the most general case, the node-voltage-based estimator is used in this thesis. The branch-current-based formulation is not suggested unless one faces an actual barrier in terms of processor for very large systems. Even in that case, the branch-current-based algorithm should be coded efficiently enough to surpass the node-voltage-based algorithms.

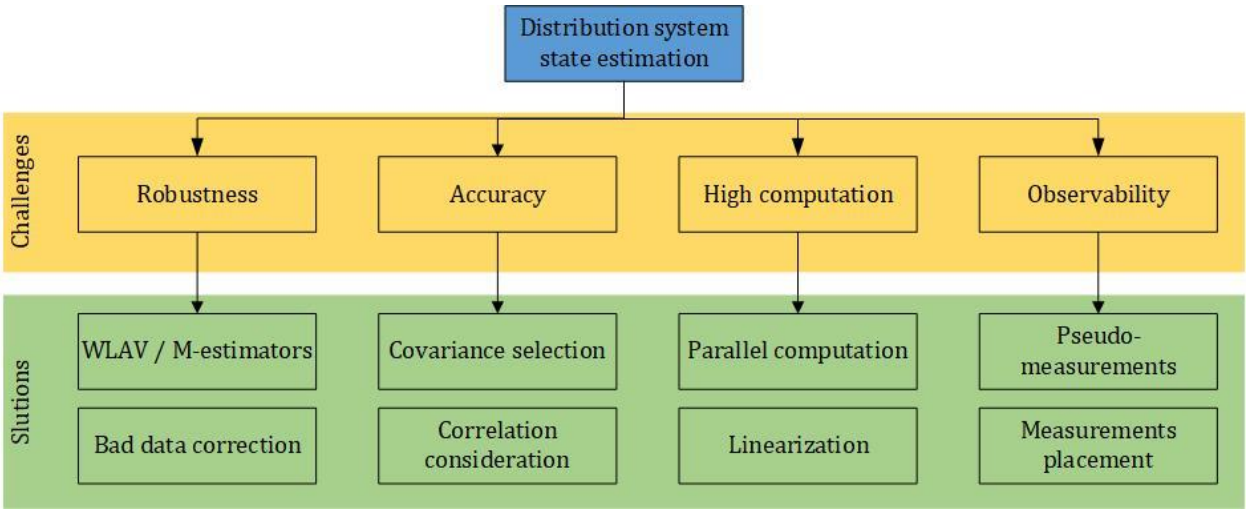

Figure 1.4 Research on distribution system state estimation: challenges and existing solutions

1.2.2.2 State estimation algorithms

From the distribution system formulations, the choice of weighted least squares (WLS) seems natural because of the very straightforward implementation on the nonlinear but static system of equations in the distribution systems, which was formulated in Schweppe's work [30].

Accordingly, many of the following research articles used WLS, unless they are trying to address other specific requirements. In general, there are three major concerns focused in this research area, which are i) the complexity of the estimation algorithm for computation and implementation, ii) the robustness and accuracy of the state estimates, and iii) system observability.

- Accuracy of the state estimates and robustness against false data

In order to cope with the false data in the measurement (measurement outliers) as an example, weighted least absolute value (WLAV) is used [33]. Alternatively, the robust M-estimators are used frequently for the same purpose [34], [35], which have more flexibility due to selection of Huber function. The M-estimators was also proposed originally in the very first days in [36]. A comparison between the WLS, WLAV and M-estimators is provided in [37]. Least trimmed squares estimator is also proposed for robustness against outliers in [38]. Others simply used the residual-based bad data detection to find and remove the measurement outlier directly [39]. The papers [33]-[39] try to deal with the measurement outliers, which are quite common in the distribution system due to the nature of the monitoring systems (low-measurement updating rate, frequent communication failure, frequent faults, voltage sag/swells or other events during which the measurements' values are biased).

- Computational requirements improvement of estimators

On the other hand to reduce the computational burden of the distribution system state estimation, different algorithms are proposed. In general, there are two approaches for computation improvements, which are different linearization of the nonlinear equations, and parallelizing the solution to large systems of equations (distributed). For example, all of the variables and equations are extended by their first two Fourier terms around the voltages 1 and angle zero prior to be used in the WLS in [40], which gives a very straightforward linear SE formulation, although it might

result in high errors. Some other linearized formulations are proposed in [41]. State estimation is formulated as a linear programming problem in [42]. In order to reduce the computations, the parallel solutions to the measurement equation is used in [43]-[44] instead of the simultaneous WLS solution. In [45], the parallel computing-based algorithm is proposed to solve WLS.

- Observability

The main challenge in the distribution system for operators is the system observability, because the system has many states that are to be monitored. Thus the number of measurements has to be ideally greater than the number of states, which is highly costly for the operators. Alternatively, the statistically stable loads can be forecasted by their daily/yearly load profiles, which are called pseudo measurements. Originally, the observability of the static system of equations is defined as a binary criterion [46]. The system is observable if the measurement matrix is invertible, and it is unobservable otherwise. However, this definition is not enough to evaluate the degree of observability. Some criteria are defined in [47]-[48], which associate a value to each measurement and thus to the overall system of measurements, depending on the contribution of each measurement error in the final estimation error. The criteria proposed in [47]-[48] are intended originally to evaluate the security of the measurements against the intrusion, which are closely equivalent to the system observability. In other words, the degree of the system observability can be evaluated using the criteria proposed in [47]-[48]. The different (sub)optimal measurement placement algorithms are proposed [49]–[51] to improve the system observability, and the estimation robustness and accuracy in turn. To cope with the lack of sufficient observability in some large systems, the game-theoretic approach is proposed in [52] that generates the pseudo-measurements from the historical data, and thus increases the accuracy of the estimates.

1.2.3 Proposed HIF detection based on existing online measurement schemes

Now we can propose the HIF detection using the introduced monitoring infrastructure. Despite the existing HIF detection schemes that use the transient high-frequency properties of HIF, we only use the static properties of HIF for detection. The proposed approach, however, analyzes the measurements from all over the distribution system simultaneously to conclude the existence and location of the HIF. The basic idea comes from the fact that the measurements from all over system are consistent within the system model, consisting of the three-phase power flow equations of the system. Thus, the accurate knowledge of the distribution system model, i.e. the values of the three-phase feeders' impedances, is of vital importance in successful performance of the proposed method. The existing and the proposed HIF detection schemes are drawn in figure 1.5.

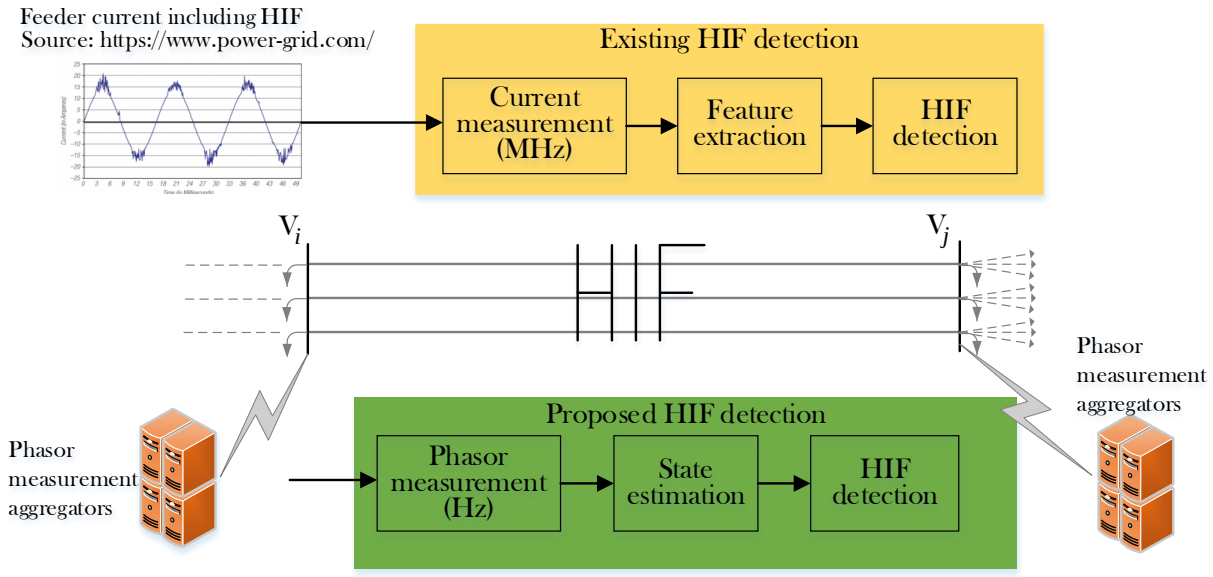

Figure 1.5 Existing and proposed HIF detection schemes

Modern distribution system monitoring based on SCADA, PMU or smart meters (or a mixture of them) provides various functionalities, such as fault detection [53], topology identification [54], energy theft detection [55], operation under communication loss [56], model

error correction [57], etc. The measurements used in the static DS-SE are able to sense the effective voltage and currents and average powers regardless of their waveform. Thus, in this thesis, the constant impedance of the HIF is considered as a model parameter to be estimated, and is augmented into the state vector of the DS-SE model. The proposed framework must be viewed as a preventative step to the surveyed literature. In other words, while the surveyed works [1]-[21] are concerned with HIFs at their worst state causing arcs or safety issues; the proposed static framework aims at locating the points of the system with high-impedance leakage without any arcs or immediate safety issues, which can replace or help with the periodical insulation tests performed in DS. To clarify the proposed framework compared with the literature, we highlight that existing HIF detection methods aim at the transient nonlinear response of the HIF and use single voltage or current measurements with high sampling frequency (e.g. 15 to 107 kHz in [10], 10 kHz in [58], 3.125 MHz in [9], and so on). However, the proposed method aims at the static properties of HIF and uses voltage phasor magnitudes and average active/reactive powers at a single time instant in a static framework to detect the existence of an HIF in the DS and estimate its location. DS-SE update rate may vary from every few seconds up to 30 minutes depending on the SE structure.

Accordingly, the main contribution of this thesis compared to the state-of-the-art HIF detection is taking advantage of the developing smart grid monitoring infrastructure, already emerging in many DS, to realize the functionality of HIF detection. The proposed approach imposes almost negligible new investment and is applied through a simple modification of the existing DS-SE algorithm. Additionally, given that the proposed approach uses the static characteristics of the HIF for its detection, it can detect faults that do not yet exhibit any nonlinear transient behavior. This is not possible for other HIF detection methods, which are mainly dependent on extracting the transient and nonlinear properties of HIF from high-resolution measured waveforms. The proposed

approach can as such enable several advantages without requiring significant new installation or investment. The proposed approach can predict the vulnerable points in the DS and give an insight to the DS operators on the susceptibility to possible events; help with or replace the periodical insulator tests for critical areas in the DS; prevent serious safety and security issues by reporting potential HIF locations to the DS operators. These advantages can collectively help with reducing the total DS maintenance costs. Furthermore, the use of Friedland's bias filter is proposed to solve the HIF-augmented SE problem. It is worth here noting that through the use of this filter the proposed approach does not require any additional measurements to preserve the system's observability after modifying the SE to allow for HIF detection. On the other hand, using traditional estimators would have required additional measurements equal to the number of the lines suspected of having an HIF, because the HIF parameters are augmented in the states vector each element of which requires an independent measurement equation to stay observable. Whereas the proposed bias filter takes advantage of the linear dependence of the augmented HIF parameters to the original system states to maintain the observability of the system without requiring more measurements.

Chapter 2: Distribution system model and state estimation

2.1 Overview

The most important parameter that determines both the performance and the cost of implementing the distribution system online monitoring is the sampling or updating rate of the measurements. In the recent years, the modern approach to online monitoring of the distribution system is a compromise between the economic and the practical aspects of the system implementation, which remains within the feasible economic boundaries of the system operation while satisfying many of desired monitoring functionalities. The sampling rate of the measurements are agreed to vary from 1 sample per 30 minutes in SCADA measurements systems or smart-meter-based monitoring, up to 60 samples per seconds in PMU-based monitoring systems, where the measurements are represented in the phasor form. Many different functionalities are proposed that are possible by this monitoring infrastructure ranging from system model identification to energy theft detection. We use the same monitoring infrastructure to enable the HIF detection, since especially the existing HIF detection methods require an economically infeasible infrastructure. Hence, in this section, the existing modern distribution system monitoring is introduced and the mathematical requirements for system state estimation is recalled. Then the HIF influence is modeled inside the existing distribution system monitoring framework, which is compatible with PMU-, SCADA-, or smart meter based monitoring of the distribution systems. Finally, we also propose use of a bias filter as the state estimation algorithm, which reduces the number of required measurements for HIF detection compared to conventional state estimation approaches.

2.2 Distribution system mathematical model

Before discussing the practical aspects of the proposed HIF detection approach, the required mathematical foundation of the distribution system model is discussed in this chapter. The proposed HIF detection approach analyzes the consistency of static measurements from all over the distribution system within the system model, to infer the existence and location of HIF. Therefore, the distribution system model, consisting of the power flow equations, is first introduced in subsection 2.1. The HIF is integrated as a static impedance parameter in the distribution model in subsection 2.2. Then, the system model is used to estimate the states of the system from the measurements. The state estimation is introduced in subsection 2.3. The states are assumed in this thesis to be node voltages magnitudes and angles in polar form. Some references used different state definitions, e.g. node voltages in rectangular form or branch current in polar or rectangular forms. The static state estimation approach to estimate the states of the distribution system allows the detection and location of HIF. The proposed HIF detection and location approach is developed in the next chapter.

The phasor representation of the electrical variables allows simplified analysis of the power systems in static framework, which are briefly introduced here. A function of time with cosine waveform with the amplitude $\sqrt{2}A$ and phase delay φ, $\sqrt{2}A\cos(\omega t+\varphi)$, is simply represented by a complex phasor $A\angle\varphi$. For voltage and currents the effective (i.e. RMS) values are used and for active and reactive powers, the average values are used in the phasor representation. The effective value of a sinewave with the amplitude $\sqrt{2}A$ is A. The more details on phasor representation are found in [59]. Since the proposed approach is purely based on the static framework, all the variables (i.e. voltages, currents, powers, impedances and admittances) are used in phasor representation.

The distribution system is modeled by assuming a subset of variables as the states and the rest of the variables as the dependent variables. Different state definitions are tried in the literature that have cons and pros compared to each other. For example, the three-phase branch currents are used as the system states in [31], and the node voltages are calculated from the branch current in each iteration. The authors of [31] claim that the branch-current based modeling of distribution system results in the sparse system model matrix, which reduces the overall computations. However, the branch current based model requires transforming the branch currents into the node voltages at the end of each iteration and transforming back the voltages to the branch current at the start of the new iteration, which significantly adds up to the complexity of the algorithm. Although the overall computation time of the branch current based models could be less than node voltage-based model, the complexity of algorithm is itself a negative aspect that can cause troubles, for example, in updating the algorithm or adding new features to the model. Therefore, the node voltage-based model of the distribution system is still the most straightforward model as proposed by Shweppe *et al* [30], which is extended in this thesis to the three-phase model.

Therefore, the three-phase complex node voltage phasors in the polar form are considered as states, from which all other variables of the distribution system can be calculated. The knowledge of the system model, i.e. the three-phase branch impedances, is of course assumed to be known by operator. The equations relating the states to the dependent variables, as well as the system model, are all static equations and parameters. Therefore, we obtain a static model of the distribution system, which allows analysis of any snapshot of the system measurements at any given time independent from the prior or posterior time instants. The definition of states, dependent variables and system model parameters, used in this thesis, are given in Table 2.1, and the notations are defined in Table 2.2.

States	Dependent variables	Model parameters
V_i^{abc}, δ_i^{abc}	P_i^{abc}, Q_i^{abc}, P_{ij}^{abc}, Q_{ij}^{abc} I_{ij}^{abc}, α_{ij}^{abc}	$\tilde{Z}_{ij}^{abc} = R_i^{abc} + jX_i^{abc}$ $\tilde{Y}_{ij}^{abc} = Y_{ij}^{abc}\angle\theta_{ij}^{abc}$

Table 2.1 Distribution system mathematical model definitions used in this thesis

Notation	Definition
V_i^{abc}, δ_i^{abc}	Three-phase voltage magnitude and angle of node *i*
P_i^{abc}, Q_i^{abc}	Three-phase active and reactive injected power of node *i*
P_{ij}^{abc}, Q_{ij}^{abc}	Three-phase active and reactive flow power at branch *i-j*
I_{ij}^{abc}, α_{ij}^{abc}	Three-phase current magnitude and angle at branch *i-j*
$\tilde{Z}_{ij}^{abc}$	Three-phase impedance matrix of branch *i-j*
$\tilde{Y}_{ii}^{abc}$	Three-phase admittance of node *i*
$\tilde{Y}_{ij}^{abc}$	Three-phase mutual admittance between node *i* and *j*

Table 2.2 Notation of variables and parameters

A 4-wire distribution system can be modeled by the three-phase representation of the system variables using Kron's reduction [60]. Then, the three-phase voltages, currents and powers are used as the system variables, which are 3 by 1 column vectors. The three-phase impedance is a 3 by 3 matrix, consisting of the branches series impedance on the diagonal elements and the mutual impedances between the branch pairs on off-diagonal elements. The three-phase admittance matrix should be calculated from the inverse of branch impedances and the system connections. Usually, the system data are provided by the branches' impedance per length unit.

The formation of the three-phase admittance matrix from the branch impedances is similar to the single-phase representation of power system, with small differences. Therefore, the formation of the admittance matrix is written here explicitly for interested readers who want to implement the proposed algorithm.

$$\tilde{Y}_{bus} = \begin{bmatrix} \sum_{i=1}^{N} Y_{i1}^{abc} & -Y_{12}^{abc} & \cdots & -Y_{1N}^{abc} \\ -Y_{12}^{abc} & \sum_{i=1}^{N} Y_{i2}^{abc} & \ddots & -Y_{N2}^{abc} \\ \vdots & \ddots & \ddots & \vdots \\ -Y_{1N}^{abc} & -Y_{N2}^{abc} & \cdots & \sum_{i=1}^{N} Y_{iN}^{abc} \end{bmatrix} \tag{2.1}$$

$$\tilde{Y}_{ij}^{abc} = (\tilde{Z}_{ij}^{abc})^{-1} \tag{2.2}$$

It can be seen that the equation (2.1) is quite similar to the single-phase formation of the admittance matrix, where only the admittance of each node and branch is replaced with the three-phase admittance. The three-phase admittance of the branch *i-j* can be simply calculated as the inverse of the impedance of branch *i-j* (2.2). However, it should be noted that for the non-existing phases, i.e. the single- or double-phase branches, the three-phase impedance should be reduced to single- or double-phase prior to inversion, which puts zeros in place of the admittance of the non-existent phases instead of infinite admittances. Therefore, the single- and double-phase branches should be identified and treated accordingly prior to implementation of the distribution system model. By having the bus admittance matrix from (2.1), the dependent variables can be written in terms of the states as following [60].

$$P_i^p = \sum_{\substack{j=1 \\ j \neq i}}^{N} \sum_{t=a,b,c} \begin{pmatrix} v_i^p Y_{ij}^{pt} v_i^t \cos(\delta_i^p - \delta_i^t - \theta_{ij}^{pt}) \\ -v_i^p Y_{ij}^{pt} v_j^t \cos(\delta_i^p - \delta_j^t - \theta_{ij}^{pt}) \end{pmatrix} \tag{2.3}$$

$$Q_i^p = \sum_{\substack{j=1 \\ j\neq i}}^{N} \sum_{t=a,b,c} \begin{pmatrix} v_i^p Y_{ij}^{pt} v_i^t \sin(\delta_i^p - \delta_i^t - \theta_{ij}^{pt}) \\ -v_i^p Y_{ij}^{pt} v_j^t \sin(\delta_i^p - \delta_j^t - \theta_{ij}^{pt}) \end{pmatrix} \tag{2.4}$$

where P_i^p and Q_i^p are, respectively, the injected active and reactive powers into the node *i* at phase *p*. Similarly other dependent variables can be calculated only in terms of system states, V_i^{abc} and δ_i^{abc}, and the system model parameters, Y_{ij}^{abc} and θ_{ij}^{abc}, as given in equations (2.5) to (2.8).

$$\begin{aligned} P_{ij}^p = {} & v_i^p Y_{ij}^{pt} v_i^t \cos(\delta_i^p - \delta_i^t - \theta_{ij}^{pt}) \\ & -v_i^p Y_{ij}^{pt} v_j^t \cos(\delta_i^p - \delta_j^t - \theta_{ij}^{pt}) \end{aligned} \tag{2.5}$$

$$\begin{aligned} Q_{ij}^p = {} & v_i^p Y_{ij}^{pt} v_i^t \sin(\delta_i^p - \delta_i^t - \theta_{ij}^{pt}) \\ & -v_i^p Y_{ij}^{pt} v_j^t \sin(\delta_i^p - \delta_j^t - \theta_{ij}^{pt}) \end{aligned} \tag{2.6}$$

$$I_{ij}^p = \text{abs}\left\{\frac{P_{ij}^p + jQ_{ij}^p}{V_i^p \angle \delta_i^{abc}}\right\} \tag{2.7}$$

$$\alpha_{ij}^p = \text{angle}\left\{\frac{P_{ij}^p + jQ_{ij}^p}{V_i^p \angle \delta_i^{abc}}\right\} \tag{2.8}$$

It can be seen from equations (2.3) to (2.8) that once the voltage magnitudes and angles are estimated, then the rest of the system variables can be directly calculated from straightforward explicit equations. However, it is not the case when the branch currents are considered as the system states, where the back and forth transformation from currents to voltages are required between each separate relations.

2.3 Integrating high-impedance fault in static model of distribution system

The possibility and validity of modeling HIF as a constant impedance will be discussed in the next chapter. In order to keep the required equation for implementation of the proposed algorithm, the constant impedance model of HIF is introduced in this subsection.

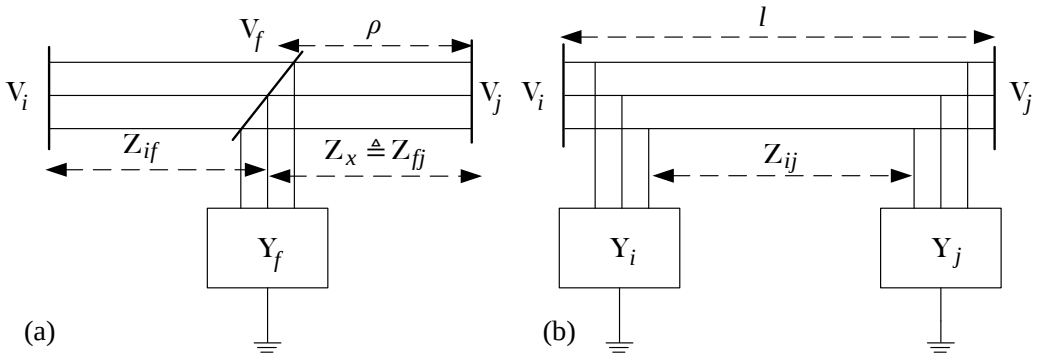

Figure 2.1 HIF static model in distribution system (a) actual HIF model (b) equivalent π-model

HIF can happen at any point of the distribution feeder. It can be seen in figure 2.1(a) that to analyze the voltage and current variables of HIF, one requires defining a hypothetical node at the HIF location, which is primarily unknown. Therefore, using the actual T-model for analyzing the HIF pose more troubles than proposing a solution. Alternatively, the equivalent π-model can be calculated for the HIF as shown in figure 2.1(b), which is derived in what follows.

2.3.1 Transformation between actual T-model and equivalent π-model

As shown in Fig. 1(a), the three-phase line impedance between nodes *i* and *j* is divided by the HIF location, in which impedances are defined as in (1).

$$Z_{ij} = Z_{if} + Z_{fj} \tag{2.9}$$

$$Z_{if} = \frac{l-\rho}{l} Z_{ij} \text{ and } Z_{fj} = \frac{\rho}{l} Z_{ij} \tag{2.10}$$

$$a = \frac{l-\rho}{\rho} \tag{2.11}$$

where *l* is the length of the feeder between nodes *i* and *j* and ρ determines the HIF location. The superscripts *a, b* and *c* pointing out the phases are omitted for readability, however, it should be noted that the impedances in figure 2.1 and those in equations (2.9) and (2.10) are the three-phase impedances of the according branches. In this thesis, where the voltage, current, power, impedance

or admittance has no superscript, it is pointing to the three-phase according variables, which are the 3 by one vectors for the voltage, current and powers, and 3 by 3 matrices for the impedances and admittances. By this notation, Z_{ij} is thus the three-phase impedance between nodes *i* and *j*, and Z_{if} and Z_{fj} are three-phase impedances between HIF location and the two side nodes. *a* is defined as in (2.11) to simplify the notations. Hence, Z_{if} is *a* times Z_{fj} in (2.10).

Writing the KVL and KCL in T-model gives equations of (2.12), where the direction of I_{ij} is from node *i* towards node *j*.

$$V_i = V_f + Z_{if} I_{ij} \tag{2.12}$$

$$V_f = V_j - Z_{fj} I_{ji} \tag{2.13}$$

$$I_{ij} + I_{ji} = Y_f V_f \tag{2.14}$$

where I_{ij} and I_{ji} are three-phase line currents at the two nodes in opposite directions. In order to simplify the derivation of formulations and highlighting the difference between the impedances of the two sides of the HIF, we call the right-side impedance of the HIF as $Z_x \triangleq Z_{fj}$, and we write the equations in terms of Z_x. By simplifying the equations (2.12) to (2.14), one can derive the relation between the three-phase voltages and currents of the two nodes *i* and *j* as written in (2.15).

$$\begin{pmatrix} V_i \\ I_{ij} \end{pmatrix} = \begin{pmatrix} A & B \\ C & D \end{pmatrix}_T \begin{pmatrix} V_j \\ I_{ji} \end{pmatrix} \tag{2.15}$$

$$A_T = I + aZ_x Y_f$$

$$B_T = -Z_x((a+1)I + aY_f Z_x)$$

$$C_T = Y_f$$

$$D_T = -(I + Y_f Z_x)$$

where *I* stands for the identity matrix of according size (3 by 3 here). Deriving equation (2.15) from the KVL and KCL equations of (2.12) to (2.14) follows a simple reordering of equations.

Now we follow the same procedure, to find the relation between the currents and voltages of the two nodes in the π-model. From figure 2.1(b), the KVL and KCL equations can be written as follows.

$$V_i = Z_{fj} I_{line} + V_j = Z_x I_{line} + V_j \tag{2.16}$$

$$I_{ij} = I_{line} + Y_i V_i \tag{2.17}$$

$$I_{ji} = -I_{line} + Y_j V_j \tag{2.18}$$

where direction of I_{line} is assumed from node *i* towards node *j*. By simplifying the equations (2.16) to (2.18), one obtains the relation between the three-phase voltages and currents of the two nodes *i* and *j* as written in (2.19).

$$\begin{pmatrix} V_i \\ I_{ij} \end{pmatrix} = \begin{pmatrix} A & B \\ C & D \end{pmatrix}_{\pi} \begin{pmatrix} V_j \\ I_{ji} \end{pmatrix} \tag{2.19}$$

$$A_\pi = I + Z_{ij} Y_j$$

$$B_\pi = -Z_{ij}$$

$$C_\pi = Y_i + Y_i Z_{ij} Y_j + Y_j$$

$$D_\pi = -(I + Y_i Z_{ij})$$

where the line impedance Z_{ij} is (a+1) times Z_x in T-model. Since the HIF admittance is relatively small, the equivalent admittances Y_i and Y_j can be found by equaling the matrices *A* and *D* in *π*-model and T-model, which yields (2.20).

$$Y_i = \frac{1}{a+1} Y_f \quad \text{and} \quad Y_j = \frac{a}{a+1} Y_f \tag{2.20}$$

The admittances Y_i and Y_j obtained in equation (2.20) are equivalent HIF admittances that are transformed from the original T-model to the equivalent π-model. It will be seen that working with the equivalent π-model of the HIF is much more comfortable than the T-model. Therefore, the problem of HIF detection is to determine the two equivalent HIF admittance in the π-model, and

then transforming back the equivalent π-model to the original T-model to determine the HIF location.

2.3.2 Power loss calculation at the HIF location

The three-phase power dissipated at the HIF location can be calculated from the three-phase complex voltage at HIF location and the HIF complex admittance, as written in equation (2.21).

$$S_{ij}^{f} = V_f \odot (Y_f V_f)^* \tag{2.21}$$

where S_{ij}^{f} is the three-phase apparent dissipated power of the HIF on the line between nodes *i* and *j*. The "⊙" product stands for the element-wise multiplication operator, different than normal matrix multiplication, and the superscript star "*" stands for the complex conjugate operator. The equation (2.21) is, however, written based on the T-model, whose parameters are not known. In fact, were we forced to use the T-model, hypothetical nodes had to be defined on each and every line of the system to represent the possible HIF locations to be estimated. However, by transforming the T-model into the π-model, we eliminated the need for additional node definition. In the π-model, we instead assume the transformed equivalent admittances of HIF onto the two side nodes of the HIF as the HIF model. In other words, an HIF on the line *i-j* is represented by two shunt admittances placed on node *i* and node *j*. Hence, the HIF's three-phase apparent power can be calculated from the equivalent π-model parameters as written in (2.22).

$$S_{ij}^{f} = V_i \odot (Y_i V_i)^* + V_j \odot (Y_j V_j)^* \tag{2.22}$$

The active and reactive flow powers of the branch *i-j* is calculated in equations (2.5) and (2.6), which are for the healthy feeders without any HIF written in terms of the active and reactive powers in real form. For derivation of the HIF influence, we repeat those formulation in complex form here as equation (2.23) and (2.24) for the two opposite side flows.

$$S_{ij} = V_i \odot I_{ij}^* = V_i \odot (Z_{ij}^{-1}[V_i - V_j])^* \quad (2.23)$$

$$S_{ji} = V_j \odot I_{ji}^* = V_j \odot (Z_{ij}^{-1}[V_j - V_i])^* \quad (2.24)$$

Now, considering that an HIF exists on the line between the nodes *i* and *j*, the flow power equations must be modified to account for the influence of the HIF in the system model. In the π-model, the influence of the HIF will be easily added to the power equations, since the two terms in equation (2.22) add up to powers of the two side nodes, which are written in (2.25) and (2.26).

$$S'_{ij} = V_i \odot I_{ij}^* = V_i \odot ([Z_{ij}^{-1} + Y_i]V_i - Z_{ij}^{-1}V_j)^* \quad (2.25)$$

$$S'_{ji} = V_j \odot I_{ji}^* = V_j \odot ([Z_{ij}^{-1} + Y_j]V_j - Z_{ij}^{-1}V_i)^* \quad (2.26)$$

Equations (2.23) and (2.24) are equivalent to the equations (2.5) and (2.6) after considering the influence of the HIF in the model. By comparing (2.25) and (2.26) to the original flow power equations (2.23) and (2.24), one notices that the influence of the HIF appears only as two apparent power terms that are added to the flow powers of its two sides. If we call the influence of HIF power on the equations as ΔS, it can be separately calculated from the $S'_{ij} - S_{ij}$ and $S'_{ji} - S_{ji}$. Now, equations (2.27) and (2.28) clearly show how to derive the influence of HIF in the system model.

$$\Delta S_{ij} = V_i \odot (Y_i V_i)^* \quad (2.27)$$

$$\Delta S_{ji} = V_j \odot (Y_j V_j)^* \quad (2.28)$$

In the state estimation model, equations (2.25) and (2.26) will be used. However, to see the influence of HIF in the power flow calculations, the admittance matrix can be simply modified as equation (2.29).

$$Y_{bus}^{f} = Y_{bus} + \Delta y \text{ where } \Delta y = \begin{bmatrix} \ddots & 0 & \cdots & 0 & 0 \\ 0 & Y_i & & 0 & 0 \\ \vdots & & \ddots & \vdots & \\ 0 & 0 & \cdots & Y_j & 0 \\ 0 & 0 & & 0 & \ddots \end{bmatrix} \quad (2.29)$$

In other words, the influence of an HIF on the line between the nodes *i* and *j* can be seen in the power flow model as the two equivalent admittances added to the according diagonal elements of the bus admittance matrix. The said modification is for the power flow calculations, however, such modification is not sufficient for the state estimation model and equations (2.25) and (2.26) must be used.

2.4 Distribution system state estimation

Depending on the measurement infrastructure in distribution systems, different types of measurements are available. Any selection of the states or dependent variable can be used as measurement in distribution systems (see Table 2.1). For example, a PMU usually measures the complex voltage of the node it is installed on, as well as the flow complex powers of the branches connected to the PMU node. In SCADA measurement infrastructure, the nodes injected active and reactive powers are measured, as well as the voltage magnitudes. Sometimes, the PMUs provide the branch currents instead of the branch flow powers. State estimation is the problem of estimating the system states from any available measurement combination from all over the system. To do so, we put all of the available measurements in a vector called measurement vector *z*.

$$z = \begin{bmatrix} V_i^{abc} & \delta_i^{abc} & P_i^{abc} & Q_i^{abc} & I_{ij}^{abc} & \alpha_{ij}^{abc} \end{bmatrix}^T \quad (2.30)$$

Equation (2.30) shows an example of the measurement vector that includes many different types of measurements. We define the state vector as the voltage magnitudes and angles, as written in (2.31).

$$x = [V_i^{abc} \quad \delta_i^{abc}]^T \quad \forall i = 1, \dots, N \tag{2.31}$$

where *N* is the number of nodes in the system. Then the measurements *z* can be written in terms of the states *x*, using the equations provided in equations (2.3) to (2.8). One writes all of the measurements in terms of the states in compact form as a vector function given in equation (2.32).

$$z = h(x) + \omega \tag{2.32}$$

where ω is the measurement error vector. State estimation problem is defined as finding the most likely state estimates $\hat{x}$ from the noisy measurements *z*. To do so, one requires first the linearization of the measurement function (2.32) by partial derivatives of all of the equations with respect to all of the states. By defining the Jacobian matrix $H = \nabla h(x)$, as the partial derivatives of the measurement function $h(x)$ w.r.t. the states, the states estimates can be found using the iterated weighted least squares (WLS) estimation from equation (2.33).

$$\hat{x}^{k+1} = (H^T W H)^{-1} H^T W (z - h(\hat{x}^k)) \tag{2.33}$$

$$H = \nabla h(x)$$

where *W* is the weighting matrix consisting of all zeros on off-diagonal elements and weights of the measurements on the corresponding diagonal elements. The weight matrix is usually considered equal to the inverse of the measurement error covariance matrix, which results in higher weights for the more accurate measurements.

2.4.1 Modeling HIF in distribution system state estimation with constant admittance

For simplicity, only the SCADA-based measurements are assumed in the simulations of this thesis, which consists of the voltage magnitude measurements as well as the active and reactive power injections, as written in equation (2.34).

$$z = \left[V_{i_v}^{abc} \quad | \quad P_{i_p}^{abc} \quad Q_{i_p}^{abc}\right]^T \quad i_v \in \Psi\,, \quad i_P \in \Phi \tag{2.34}$$

where Ψ is the set of the nodes with voltage magnitude measurements, and Φ is the set of the nodes with power injection measurements. Now, in order to integrate the HIF detection in the state estimation problem, we define an augmented states and HIF parameters vectors as written in (2.35).

$$x^f = [x \quad \beta]^T \tag{2.35}$$

where x^f is the augmented state vector with the HIF parameters, and β is the vector of the HIF admittance parameters defined in (2.36).

$$\beta = \begin{bmatrix} Y_i^a & Y_i^b & Y_i^c & Y_j^a & Y_j^b & Y_j^c \end{bmatrix}^T \tag{2.36}$$

We write the measurement equations now in terms of the states and the augmented parameters β as given in (2.37).

$$z = h(x) + m(x, \beta) + \omega \tag{2.37}$$

where *m*(.) is the measurement model adjustment vector function, which consists of all zeros for all of the voltage measurements as well as the power measurements of all nodes except for the power measurements of nodes *i* and *j* (the two side nodes of the line that has HIF). Model adjustment vector function due to HIF can thus be obtained from equations (2.27) and (2.28). Therefore, the model adjustment *m*(.) due to HIF can be obtained from equation (2.27) and (2.28) for the injection power measurements at nodes nodes *i* and *j* and zero for all other power and voltage measurements as in (15). It is worth noting that if the flow power measurements were assumed, the corresponding model adjustment function could be obtained from (2.27) and (2.28), where only the flow measurements of the HIF line have non-zero adjustment. In general, an HIF on line *i-j* results in non-zero model adjustments of only measurements: P_i^{abc}, Q_i^{abc}, P_j^{abc}, Q_j^{abc}, P_{ij}^{abc}, Q_{ij}^{abc}, P_{ji}^{abc} and Q_{ji}^{abc}, which can be obtained from equations (2.27) and (2.28).

Now, in the assumed measurement vector (2.34) only based on SCADA measurements, the model adjustment has zero elements for all of the voltage measurements, as well as all of the active and reactive measurements except for nodes i and j. The corresponding model adjustment vector function is written in equation (2.38).

$$m_k(x,\beta) = [\cdots \quad Re\{\Delta S_k\} \quad \cdots \quad Im\{\Delta S_k\} \quad \cdots]^T \quad k \in \{i,j\} \tag{2.38}$$

By substituting (2.38) in (2.37), the measurements are written in terms of the states as well as the hypothetical HIF parameters. It will be discussed in the next chapter that which lines should be selected to augment for the HIF parameters. In order to find the states and HIF parameters' estimates from equation (2.37) simultaneously, one requires to linearize the two functions *h*(.) and *m*(.) with respect to all states and HIF parameters, which are written in (2.39) and (2.40).

$$H^f = \begin{bmatrix} \frac{\partial h}{\partial x} & \frac{\partial h}{\partial \beta} \end{bmatrix} = [H \quad \bar{0}] \tag{2.39}$$

$$M = \begin{bmatrix} \frac{\partial m}{\partial x} & \frac{\partial m}{\partial \beta} \end{bmatrix} \tag{2.40}$$

where $\bar{0}$ is the matrix of all zeros of corresponding size. Then the augmented system of states and HIF parameters (2.37) can be linearized as (2.41).

$$z^f = H^f x^f + M x^f + \omega \tag{2.41}$$

Adjusted measurement equation due to HIF is obtained finally as in (2.41), by adding H^f and *M*, called H_{adj} as (2.42), which yields the adjusted measurement equation in form of (2.43).

$$H_{adj} = H^f + M \tag{2.42}$$

$$z^f = H_{adj} x^f + \omega \tag{2.43}$$

Note that the power equation adjustments of (2.38) is the left side of matrix *M* in (2.40); in other words, the power adjustments Δp_k and Δq_k are added to the model inside the adjusted Jacobian of

(2.42). Now, having the adjusted model of (2.43), the weighted least squares (WLS) can be employed to find the estimation of augmented states and parameters similar to (2.33).

2.4.2 Modeling HIF in distribution system state estimation with constant power

The exact impedance value of HIF, as explained, is not of interest as far as its location could be identified. Therefore, the HIF's constant admittance model can be simplified to obtain a more convenient formulation of state estimation. It is noticed from (2.22) that the power of HIF is a function of its admittance and voltage magnitude, where the admittance is considered constant and voltage magnitude is subject to change but in a very limited range in the normal operation of distribution systems. Note that the HIF phenomenon still remain in the normal operation range of distribution system without violation. Therefore, it can be inferred from (2.22) that a constant power model for HIF will perform almost the same as constant admittance in the SE, while simplifying the formulations. Define the new parameter vector to be estimated as the active powers of HIF in three phases as in (2.44).

$$b = \begin{bmatrix} p_i^{abc} & q_i^{abc} & p_j^{abc} & q_j^{abc} \end{bmatrix}^T \tag{2.44}$$

where *b* is the parameter vector to be estimated (or biases as will be explained shortly), and p_i^p and q_i^p are the active/reactive powers wasted in HIF at node *i* phase *p*. By following the similar procedure as the constant admittance model, we derive the adjusted estimation model due to HIF as following. First we augment the states with the HIF parameters *b*, which are now the active and reactive powers dissipated at the HIF location, as written in (2.45).

$$x^f = [x \quad b]^T \tag{2.45}$$

By the new parameter definition *b* instead of β, the model adjustment can be calculated as (2.46).

$$m(x, b) = [\ldots \quad p_k^{abc} \quad q_k^{abc} \quad \ldots]^T \ \ \forall k \in \{i, j\} \tag{2.46}$$

The partial derivatives of the adjustment vector function of (2.46) are one with respect to the parameters *b* and is zero with respect to states *x*. Thus, the constant power model for HIF results in a significant simplification of the model adjustment matrix, which is given as following.

$$M = \left[\bar{0} \quad \frac{\partial m(x,b)}{\partial b}\right] = [\bar{0} \quad D]$$

where $\bar{0}$ is the matrix of all zeros, and *I* is the identity matrix. Comparing (2.46) to (2.40) shows the advantage of the simplified model (i.e., the constant power model of the HIF). This simplification can be appreciated the most by considering the implementation of the SE iterations, because it relaxes the updating of the elements inside the original measurement matrix *H* (as can be seen in (2.46) the derivative of model adjustment is zero w.r.t. states). Now, we can replace *M* of (2.46) instead of (2.40), to form the augmented SE problem in (2.43), which can be solved directly using WLS.

More importantly, by modeling as constant power, HIF appears as biases in the injected power measurements as derived in (2.46). Since the left-hand side of the model adjustment matrix *M* in (2.46) becomes zero for the constant power HIF model, the HIF can be modelled as measurement biases. Recall the measurement equation for a linear observable system with biased measurements as in (2.47).

$$z = Hx + Db + \omega \qquad (2.47)$$

Modeling the HIF instead of model parameters as (2.40) requires parameters and states' simultaneous estimation. However, the constant power model results in the simplified model of (2.47), which allows use of Friedland's solution to the augmented system [61], as formulated for DS-SE in [55], [56], wherein the iterative filter equations are presented. For simultaneous states and parameters estimation, for a system with *n* states, and n_s number of suspected HIF parameters, the augmented system has $n + n_s$ states and parameters, which requires a number of measurements

$m > n + n_s$ in order to be observable. However, by using Friedland's decomposition of states from biases in (2.47), $m > n$ measurements are sufficient for full observability, where the linear dependence of the biases to the existing measurements is exploited to provide the observability of HIF-augmented system, only given the observability of original system, thus reducing number of measurements by n_s. Friedland's bias filter, as written in iterative equations of (2.48), is thus used to solve the estimation problem of (2.47).

$$\hat{x}_k = \tilde{x}_k + V_k \hat{b}_k \tag{2.48.a}$$

$$\tilde{x}_{k+1} = \tilde{x}_k + \hat{K}_k r_k \tag{2.48.b}$$

$$\hat{b}_k = (I - \hat{K}_k S_k)\hat{b}_{k-1} + \hat{K}_k r_k \tag{2.48.c}$$

$$M_{k+1}^{-1} = M_k^{-1} + S_k^T (H\tilde{P}_k H^T + R)^{-1} S_k \tag{2.48.d}$$

$$S_k = HU_k + D \tag{2.48.e}$$

$$\hat{K}_k = M_{k+1}(HV_k + D)^T R^{-1} \tag{2.48.f}$$

$$S_k = HU_k + D \tag{2.48.g}$$

$$r_k = z_k - h(\hat{x}_k) \tag{2.48.h}$$

where $\hat{b}_k$ is the bias estimates, $\tilde{x}_k$ is bias-blind state estimates of standard Kalman filter and $\hat{x}_k$ is corrected estimates of states after bias correction.

The constant admittance parameters modeling of HIF, as obtained in (2.36), is a more accurate model for HIF detection and location, which could be solved using the WLS. However, augmenting the HIF parameters to the states for being estimated by WLS requires additional measurement in order to prevent unobservable system. Defining the HIF powers as the parameters to be estimated resulted in the simplified measurement function (2.47), where the HIF parameters appeared as the measurement biases and allows using the bias filter (2.48), which does not require any additional measurements. If the original system is observable, the HIF-augmented system is

also observable regardless of the number of HIF power parameters augmented into the system. However, there is one drawback in the latter simplified model that is it cannot distinguish between the HIF parameters, measurement biases or even energy theft. If the possibility of such events are at stake, the use of the constant admittance model for HIF (2.38) is thus suggested, which requires additional measurements.

The mathematical foundation of the proposed HIF detection algorithm is developed. To summarize the proposed approach, one models all the possible/suspected HIFs of the system as the constant active and reactive powers as written in (2.44), then forms the linearized measurement model as (2.47) by determining the *H* and *D* matrices from partial derivatives of the measurement function and model adjustment, respectively, with respect to states and HIF powers. Finally, the recursive bias filter, as given in (2.48), is used to estimate the states and the biases, which are HIF's constant power parameters now. The more details on possibility and validity of the proposed HIF detection approach is discussed in the next chapter.

2.5 Summary

Since the existing HIF detection approaches based on the feature extraction from the high-resolution current or power measurements are significantly expensive for the distribution system operators, we proposed using the existing distribution system monitoring infrastructure to integrate the HIF-detection functionality. The mathematical basis for the HIF modeling in the existing distribution system monitoring infrastructure is developed in this section, above all. Then we also proposed using the bias filter instead of the WLS algorithm for state estimation, which reduces the required number of measurements for the detection of HIF, by taking advantage of the linear dependence of the HIF parameters to the system states. The mathematical frameworks enables the

state estimator block to integrate the HIF detection. The more practical aspects of the proposed approach is discussed in the next chapter.

Chapter 3: HIF location procedure and considerations

3.1 Overview

In practice, the proposed methodology faces several bottlenecks in the implementation, which are discussed in this chapter. The main bottleneck of this approach, as other functionalities based on the distribution system monitoring, is the limited number of measurements in the system. In which case, augmenting all of the lines in the estimation algorithm with HIF parameters to be estimated results in a significantly reduced performance. To overcome this issue, we propose augmenting only the more suspected lines in the estimation algorithm for HIF detection. For example, a conventional number in the literature is that there are measurements in the system 1.5 times the number of states. After evaluating the proposed HIF detection approach, we compromise between the performance accuracy and the inclusion of different system locations by choosing more than half of the system branches to be observable for HIF detection. Second, the proposed approach has always a non-zero estimation for all of the HIF parameters. Thus, we propose a procedure for the distribution systems in practice to implement and calibrate the proposed algorithm which improves the performance of the proposed HIF detection. Finally, an implementation of the proposed algorithm is given, where the practical aspects are also considered.

3.2 Detection of HIF existence in the system

The HIF model and its integration into the SE is studied in the previous section. Now we discuss the implementation of the proposed method on a DS. In DS-SE a new state estimate is calculated every time-step ΔT. Typically, in DS-SE a time step varying from a few seconds to several minutes is considered depending on the load and generation volatility as well as the

acceptable computational and communication burden. On the other hand, DS-SE uses measurements of voltages, currents and powers collected from different nodes in the DS. These measurements can include measurements from SCADA units installed on the MV/LV transformer substations (updated every few seconds), measurements from smart meters installed at loads (updated every few minutes), pseudo-measurements (that can be updated as desired) or measurements from other types of phasor measurement units (updated from 1 to 60 times per second). Several research articles in the literature have already investigated detailed methodologies for accommodating measurements with different resolutions and for using unsynchronized measurements in the DS-SE [62], [63]. The integration of unsynchronized measurements and measurements with different resolutions in the DS-SE is beyond the scope of this work, and interested readers are referred to [62], [63] (and the references therein). In this work, it is assumed that the available measurements are already synchronized with the same time resolution. As such, the proposed DS-SE approach updates (i.e., calculates a new state estimate) every ΔT using measurements about the preceding time-step. For each update, the HIF-augmented DS-SE component estimates the HIF parameters, which are simplified to biases in the power measurements. Since all of the power measurement devices provide the average powers over the past time-step ΔT, the estimated HIF parameters are also the average of the dissipated power at the HIF location over the past time-step ΔT. If the value of the average power dissipated at the HIF location during the preceding ΔT is higher than the detection threshold, then the proposed algorithm detects it as a positive HIF event. In other words, the HIF parameters in (29) are the average HIF power loss over the past time-step. Accordingly, from the proposed DS-SE perspective, there is no difference between a HIF having a time-variable power with an average

$\tilde{P}_{HIF}$ and a HIF with a constant power $\bar{P}_{HIF}$. This property leads to the assumption of constant power for the HIF, and enables us to model HIF with its average power.

The model given in (24) provides estimation of parameters of HIF between the two known nodes *i* and *j*. However, the problem of HIF location is rather to find the nodes *i* and *j* in advance. In order to locate the HIF, i.e. finding *i* and *j*, a set of suspected nodes ψ is considered. The set of suspected lines is generally determined based on the DS operator's knowledge and historical records (maintenance and events) of the DS lines and their vulnerability to different phenomena. The most vulnerable lines in the DS are to be used as the suspected lines in the proposed approach. Practically, the determination of the most vulnerable lines is usually attained through the application of data analytics techniques on the maintenance and event records of the individual lines in the DS. Several research articles in the literature have already investigated methodologies for the determination of the DS's most vulnerable lines in real time based on historical data [64]–[66]. The determination of the DS's most vulnerable lines based on the historical records of the DS is beyond the scope of this work, and interested readers are referred to [64]–[66], and the references therein, for detailed methodologies on how to identify the most vulnerable lines in a DS. Typically, the lines with higher rate of recorded events are more vulnerable to HIF. Besides, the long laterals located far from the main feeder are also susceptible to HIFs. In this work, we assume that longer feeders with smaller loads at their ends are more susceptible to HIFs and the set of suspected lines is selected accordingly. Here it is worth mentioning that if we do not assume a set of suspected lines and augment the entire system for the HIF detection, the detection performance will decrease due to the high ratio of states to be estimated with respect to the measurements. Furthermore, the augmentation of parameters at the so-called bad leverage points

[67] can result in a significantly deteriorated performance of the SE. The parameter vector b is then defined as all the possible HIF's active and reactive powers in suspected nodes ψ as in (3.1).

$$b = [P_s^{abc} \quad Q_s^{abc}]^T \quad \forall s \in \psi \tag{3.1}$$

where ψ is the set of the nodes on the two sides of the lines that are suspected to have HIF. The number of the HIFs on different lines that can be estimated using one snapshot of the measurements depends on the observability degree of the system, i.e. the number and locations of the measurements in distribution system. Then the states are augmented with all suspected parameters of (3.1) and their estimation will be obtained accordingly from iterative equations of bias filter provided in (2.48).

In summary, first the bias vector is defined on all of the suspected nodes ψ, which is estimated using (2.48), and the largest elements of the estimated bias vector is assumed to be corresponding to the HIF temporarily. Then the bias vector is reduced from including all of the suspected nodes to only the *i* and *j* nodes on the two sides of the HIF (i.e. the largest estimated bias), and the estimation problem of (2.48) is run again to find the reduced bias vector estimates. The norm of the reduced bias vector is used for detection of the HIF existence via the threshold test of (3.2).

$$HIF\ existence = \begin{cases} False, & \text{if } \|b\| < \tau \\ True, & \text{if } \|b\| > \tau \end{cases} \tag{3.2}$$

The same estimation of the reduced bias vector is then used to obtain the location of the HIF. In order to realize reliable performance in determining the location of the HIF (but not necessarily for the HIF existence detection) the proposed algorithm needs calibration around the nominal condition of the healthy system (i.e., system with no HIF) to account for the intrinsic parameter errors. On the other hand, the detection of the HIF-existence performs with a high reliability without this calibration, which can be significantly improved with the calibration. In

order to demonstrate and clarify what the intrinsic parameter errors represent and how these errors affect the performance of the proposed algorithm, in the next two subsections we first explain the implementation without the intrinsic error correction mechanism and then follow that by an explanation of the implementation with the intrinsic error correction mechanism.

3.3 Without intrinsic error correction (Plan A)

If the HIF exists in line *i-j*, the values for the parameters estimates at these nodes will be considerable values with respect to parameter estimates at other nodes. By determining the nodes *i* and *j*, the line *i-j* is detected to include HIF, which is enough information for operators in most of the cases, since they should inspect the line for removal of tree contacts or insulator breakdowns. However, in case of long lines or underground networks, the exact location of the HIF can be very time- and budget-saving before starting the inspection. Therefore, after finding the nodes *i* and *j*, other suspected parameters are omitted from parameter vector, and augmented states are built on solely the two estimated nodes *i* and *j*. By reducing the parameter vector size from all suspected nodes to only two detected nodes, an accurate estimation is obtained, which can be used to exactly locate the HIF. The parameter estimation approach yields the powers of the HIF, from which its admittance can be obtained, since the system voltages are also estimated simultaneously with the HIF power parameters. Thus it gives the equivalent HIF admittances in the π-model, and using (2.20), we find *a* and the HIF distance from end node *x* as (3.3).

$$a = \frac{\|Y_j\|}{\|Y_i\|} \rightarrow \rho = \frac{l}{a+1} \tag{3.3}$$

where *l* is the length of the line *i-j*, and ρ is the HIF distance from node *j*, as shown in Fig. 1.

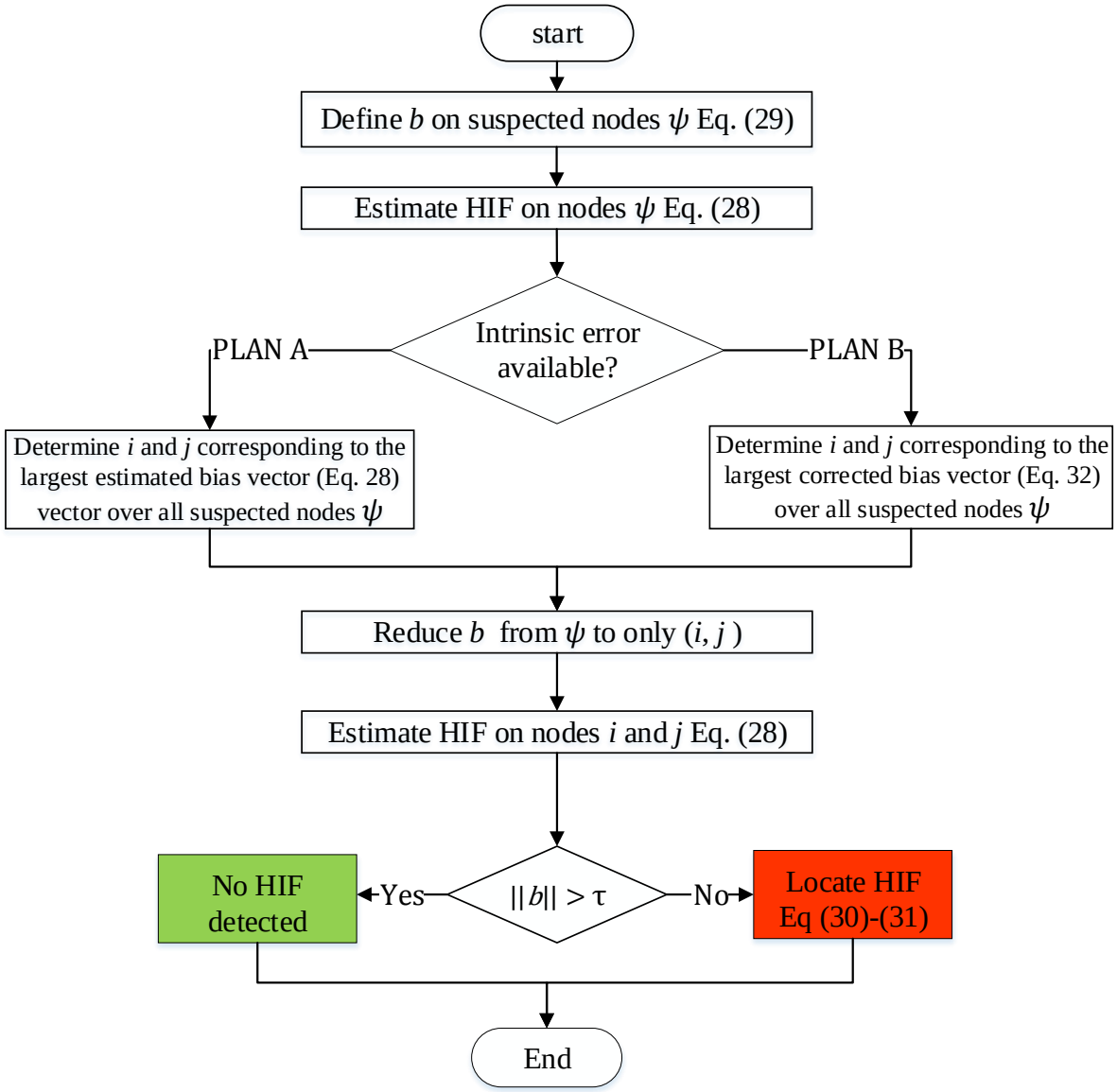

Figure 3.1 HIF detection flowchart; the intrinsic error vector *E* is the bias estimates over the suspected nodes under nominal load condition of healthy system with no HIF; Plan A and Plan B are respectively without and with the intrinsic error correction

3.4 With intrinsic error correction (Plan B)

Ideally, if the system model is perfect, the bias estimates are all zeros for a healthy system, and non-zero elements directly reflect the occurrence of an HIF. However, due to model uncertainty and linearization, the bias estimates are not zero even in a healthy condition. In this

work, we denote the errors arising from model uncertainty and linearization as the intrinsic parameter error in the system. This means that even if we formulate the proposed parameter estimation problem for a healthy DS (i.e. without any HIF), HIF parameter estimates may have nonzero values. In this thesis, we propose to account for these intrinsic parameter errors by first applying the proposed parameter estimation on the healthy system (i.e., without any HIF), and saving the estimated HIF of all suspected nodes in the vector *E*. In other words, the bias estimates $\hat{b}$ of the healthy system with no HIF is saved as *E*, which would consist of small values. The estimated values for parameters in this step do not represent any HIF, but come from intrinsic parameter errors inaccuracy. By saving the HIF parameters' estimates in the healthy system condition, a more accurate estimation of the HIF can be obtained by subtracting vector *E* from our bias estimates in the subsequent operating conditions. In other words, the HIF parameter estimates in the healthy system, that are ideally zero but have non-zero values, are the intrinsic errors of the proposed HIF estimation, around which we propose the calibration of the DS-SE. In practice, the intrinsic model error can be obtained by running proposed estimation on the system when it is newly constructed, where the possibility of the HIF and other events are minimum and the model information are accurate. If the estimation is designed for an already operating DS, there is a need for a general inspection of the system for all possible events and errors in order to get the most accurate model information. Then it is time to save the intrinsic error estimates, which should be subtracted from the subsequent HIF estimates. If the difference between the estimated value and the pre-calibrated value of bias vector (3.4) exceeds the threshold, the HIF can be detected.

$$\hat{b}_{corrected} = \hat{b} - E \tag{3.4}$$

where *E* is the vector of the intrinsic error correction, which consists of the bias estimates in the healthy system condition under nominal loading. Finally, if the estimated HIF parameters exceed

the detection threshold τ, it will be positively detected and its location is reported. The threshold is selected based on the detection performance indices shown in next section. Fig. 2 gives a flowchart summarizing the proposed HIF estimation methodology.

3.5 Observability and Measurement Placement

Observability is essential for different DS-SE functionalities. For example, DS observability is required to enable fault detection [53], topology identification [54], energy theft detection [55], operation under communication loss [56], etc. Measurement placement to realize DS observability has accordingly been extensively investigated in the literature (e.g., [68]–[70]). In this section, a simple exhaustive search algorithm is adopted for measurements placement for DS observability. The placement results realize system observability which can be used to perform HIF detection as well as other control and monitoring functionalities. Here it is worth reiterating that, as discussed in section III, the proposed HIF detection formulation does not require any additional measurements compared to performing DS-SE for any other purpose without allowing for HIFs detection. The measurement placement algorithm is based on rank of gain matrix in SE, in addition to its condition number. The rank of square matrix *G* is defined as the number of its linearly independent rows or columns. It is also equivalent to number of nonzero eigenvalues of the matrix. The condition number of a matrix *G* is defined [71] as in (3.5).

$$\mathcal{K}(G) = \frac{\sigma_{max}(G)}{\sigma_{min}(G)} \tag{3.5}$$

where σ stands for the singular values of matrix *G*.

In order to find the measurement placement, we define a placement vector including power and voltage measurements. It is considered that when there is a voltage measurement in a node, voltages of all three phases are measured. Moreover, when there is a power measurement, both the

active and reactive powers of three-phases are measured. First, we examine all possible measurements that can be added to the placement vector *C* separately and find all corresponding gain matrices *G*. The measurement with highest rank of gain matrix is selected. If there are more than one measurement that result in the maximum rank, then the measurement with the lowest condition number is selected. We repeat the procedure for second measurement and so on. Our objective is to determine the least number of measurements for system observability and ability to detect HIF. The least number of measurements are obtained after determining the first measurement that makes the gain matrix full-rank, as demonstrated in Algorithm 1.

Algorithm 1: Measurement placement

1. Initialize placement vector *C* as empty
2. Examine all possible measurements to be added to *C* separately and find all corresponding gain matrices *G*
3. Select the measurement corresponding to the gain matrix with highest rank and lowest condition number
4. Update the placement vector *C* with selected measurement
5. ***If*** *G* is full-rank ***Break***
6. ***Go to*** **2**

3.6 Summary

The proposed HIF detection approach is based on the existing distribution system monitoring infrastructure, which is used for various functionalities. Thus, instead of manipulating the existing infrastructure to enable the proposed approach, we proposed several variations in the proposed algorithm to be compatible with the existing infrastructure and its other functionalities. The two major aspects that were proposed to make the proposed approach practical, was first reducing the set of HIFs from all possible HIF in the system to only those HIF on the suspected branches of the system, and second calibrating the proposed algorithm around the HIF estimates

in non-HIF condition of the system. The other practical aspects of the proposed approach is also discussed in this chapter, such as inclusion of different types of measurements.

Chapter 4: Simulation results

4.1 Overview

In order to investigate the performance of the methodology proposed in this paper, two IEEE test systems are selected; namely, the IEEE 13-bus and 123-bus systems [46]. The results of the measurement placement algorithm are first presented to realize system observability and enable HIF detection. Random HIF cases are studied, differing in HIF impedance, line and phase containing HIF and HIF distance from sending end. The influence of load variation is also considered by choosing random load factors for different loads, which are assumed to work between 25% below and 15% above their nominal load. The simulation validation of the proposed location procedure consists of three main parts. First the existence of HIF is detected. Then the line with HIF is identified, and finally its distance from the sending end is estimated. In this work, it is assumed that longer feeders with smaller loads at their ends are more susceptible to HIFs and the set of suspected lines is selected based on this criterion to include 7 lines in 13-bus system and 70 lines in the 123-bus system, corresponding to 32 and 218 HIF parameters in 13-bus and 123-bus systems, respectively. Here it is worth mentioning, that the proposed algorithm is augmented with all of the HIFs on suspected lines. However, after positive detection of one HIF line (when its estimated value exceeds the threshold), the DS-SE start over and is augmented only with the HIF on the detected line. The latter step helps with the estimation of the HIF location more accurately. In order to compare the proposed methodology to existing work in the literature, the comprehensive literature review provided in [1], comparing the different HIF detection methodologies, is used. Specifically, the survey in [1] reports the accuracy of 21 references, and we used the average accuracy of the reported references to benchmark our results. The

measurement error is generated by random Gaussian noise with zero mean and variance 0.01 p.u. for all measurements in all cases.

The proposed algorithm is based on the DS-SE, which is dependent on the placement of the measurements throughout the system. Therefore, a simple placement algorithm is used as discussed in previous chapter, whose results are provided for IEEE 13-node and 123-node feeders in this chapter before simulating the other case studies. Then, the performance of the proposed algorithm is evaluated first in terms of detection of HIF existence in system (which is itself a valuable knowledge for operators), and then in terms of the HIF location identification of the algorithm. The proposed algorithm performs differently on different feeders of the system, which depends on the system connections and model accuracy. Therefore, at the end of this chapter, a performance criteria is defined and all of the suspected line for having HIF (7 and 70 branches in 13-node and 123-node feeder systems) are evaluated using the defined performance criteria.

4.2 Measurement placement

Results of the proposed measurement placement algorithm are presented for the IEEE 13-bus and 123-bus systems in Tables 1 and 2, respectively. It is noticed that the 13-bus system is reduced to 10 nodes after removing the switch buses and merging their terminal nodes. Among the 10 nodes, there exists three-phase as well as single- and double-phase loads and lines. The states pertaining to non-existing phases are removed from the state vector leaving the 13-bus system to be modeled with 43 states. Similarly, the 123-bus system is modeled with 497 states. In the 13-bus system, there are 8 measured nodes, among which nodes #5 and #10 are double-phase and node #6 is single-phase; the total number of measured values are 49. Similarly, there are 80 measured nodes in 123-bus system, and the total number of measured values are 529 including

voltage magnitudes, active and reactive power measurements. In addition, 2 and 41 pseudo-measurements are assumed in the 13-bus and 123-bus systems, respectively, with error variance of 30%.

13-bus system measurement placement results (measured nodes)	
Power	632 633 646 652 671 675 680 684
Voltage	632 671 675

Table 4.1 Measurement placement results for the 13-node feeder

123-bus system measurement placement results (measured nodes)	
Power	1 2 3 4 5 6 7 8 9 12 13 18 19 21 23 25 26 27 28 29 30 35 36 37 38 40 42 44 45 47 48 49 50 51 52 53 54 55 56 57 60 61 62 63 64 65 66 67 68 72 76 77 78 79 80 81 82 83 86 87 88 89 90 91 93 94 95 96 97 98 100 101 105 108 110 135 149 160 197 250
Voltage	1 13 21 25 35 47 56 60 65 67 76 80 85 88 93 98 105 111 113 150 151 250 450

Table 4.2 Measurement placement results for the 123-node feeder

4.3 Detection of HIF existence

To evaluate the detection performance of the proposed scheme, 10,000 cases are generated, half of which is the system in healthy condition (no HIF) in different load conditions, and the rest include 5000 random HIFs in different loading condition of the systems. The value of HIF considered in the literature vary from 400 Ω [3] up to 15 kΩ [4]-[6], depending on the type of HIF. The more details can be found in [3] and the references therein, where the HIF impedances are discussed for different contacts and surfaces for broken and unbroken conductor cases, respectively. In current setup, the HIFs are all considered as single-phase to ground, characterized by four random values that are impedance, line, phase and distance from the end node. The HIF

power values considered in the literature varies from 0.011 (for 15 kΩ) to 0.43 p.u. (for 400 Ω), where the base power and base voltage are 100 kVA and 4.16 kV in both 13- and 123-bus test systems. On the other hand, the individual power measurement errors in DS do not exceed 1% (or 0.01 p.u.) according to [72], and the deployed Kalman filter is the sovereign remedy for this measurement error, so the error of estimated values are far less than the individual measurement errors. Thus, if we assume the 0.01 p.u. as detection threshold, it is highly unlikely that the measurement errors in normal conditions exceed it to result in the false alarm, while it is still less than the least assumed HIF power in the literature (i.e. 0.011 p.u.).

System	Plan	Accuracy	Security	Safety	Dependability
13-bus	A*	95.87	92.85	99.26	99.31
	B**	99.75	99.50	100	100
123-bus	A	96.39	93.65	98.87	98.93
	B	99.60	99.20	100	100

Table 4.3 HIF existence detection performance in 13-node and 123-node feeders

*A: without intrinsic error correction
**B: with intrinsic error correction

There are four typical performance indices for detection evaluation: accuracy, security, safety and dependability, that are different ratios of true and false alarms for positive and negative events as precisely defined in [1], which are recalled here in equations 34(a)-(d).

$$Accuracy = \frac{TP + TN}{TP + FP + FN + TN} \tag{4.1}$$

$$Security = \frac{TN}{TN + FN} \tag{4.2}$$

$$Safety = \frac{TN}{TN + FP} \tag{4.3}$$

$$Dependability = \frac{TP}{TP + FP} \tag{4.4}$$

where TP and FP refer to true positive and false positive alarms, and TN and FN refer to true negative and false negative alarms. The four performance indices of the proposed method are reported in Table 3. In the state and parameter estimation literature, two metrics are widely used to evaluate the detection performances that are detection probability and false positive alarm (see [48]-[50] for example). The detection probability can be inferred from the dependability and accuracy, while the false alarm rate can be interpreted to security and safety. It can be seen from Table 3 that if the intrinsic error correction is implemented, the detection of HIF existence is very accurate. The results of HIF existence detection is also reliable even without the intrinsic error correction.

4.4 HIF line identification

In this section, we investigate the capability of the proposed approach to correctly identify the lines containing the HIF. To this end, several possible values of the HIF impedance are considered (varying from 400 Ω to 15 kΩ). A 1000 runs of simulation are performed with each value of the HIF impedance, where in each run a line is selected randomly from the set of suspected lines to include an HIF. The statistics of successful identification for the different HIF impedance values (computed over each 1000 runs), are then reported under the base load case in tables 4 and 5, for the 13-bus and 123-bus systems, respectively. Subsequently, in order to also assess the capability of the proposed approach to accurately identify the line with an HIF at off-nominal load conditions (i.e., when the system loads are not at their nominal values), different cases are

considered wherein individual loads are multiplied by different random load factors in each run. Two different ranges of load factors are considered (i.e., [-15%, +10%] and [-25%, +15%]), and additional runs are performed for each of these load factor ranges. In the proposed model, HIFs can be more easily detected if the system is close to no-load conditions, e.g. during night, because of higher influence of the HIF in the measurements. On the other hand, the nominal loads in the DS are the maximum desired loads, exceeding from which may lead the system to its stability limits, thus the loads variation range is selected not to exceed more than 15% above and reduced below 25% the nominal load. The statistics of successful identification for the different HIF impedance values (computed over each 1000 runs) are then reported in tables 4 and 5, for the 13-bus and 123-bus systems, respectively. The consideration of random load variation, enables us to test the validity of the proposed HIF detection approach under practical load variations, due to the unknown nonlinearity of the system model with respect to load variations. The simulation results confirm such nonlinearity showing decreased performance for larger load variations. Yet in the assumed range of load variations, the algorithm gives acceptable detection of the HIF.

Besides, the influence of load balancing is also considered to test the detection algorithm. In the 13-bus system, the nodes 645 and 646 have single-phase load while they are fed through double-phase lines. Node 675 has a significantly unbalance load with 485 kW, 68 kW and 290 kW on phases a, b and c, which can also be divided equally between the three-phases if the required switching equipment are deployed. Although the loads of node 671 are unbalance, they are 402 kW, 451 kW and 672 kW for a, b and c phases, and also this node is upstream feeder of the nodes 611, 652, 684, 680 and 675, and the cumulative loads for the three-phases is approximately balance at this node. Therefore, load balancing is considered only at the nodes 675, 645 and 646 in the 13-bus system. Similarly, there are 80 single phase loads in the 123-bus system, among which 28

nodes are connected to a three-phase feeder and two of them connected to double-phase feeders. The load-balancing is assumed only on the 28 nodes, in each run a percentage of these nodes are randomly selected, and their loads are equally divided between the three-phases. In other words, in each run a percentage of the single phase loads are selected and their loads are divided between their three phases equally. Two cases are assumed here that are 33% and 67% of the nodes (with single-phase load) are subject to load-balancing. Additionally, line outage and re-energization may happen frequently in DS due to faults or maintenance. It was discussed that the transient behavior of such events might have negative influence on the DS-SE but only for the results of the measurement interval during which the events happened. Besides, the line outage event deviates the system model from the original model around which the bias estimates are calibrated in the proposed approach. Therefore, the influence of a single line outage is also assumed in the simulation, where one line is removed from the network in each run. The influence of single line outage on the proposed HIF detection is also reported in Tables 4 and 5 for the 13-bus and 123-bus systems, respectively.

Load		Plan	400 Ω	800 Ω	1.2 kΩ	5 kΩ	15 kΩ
Base load		A	87.9	82.9	73.2	63.2	55.8
		B	99.8	99.6	99.6	98.8	98.2
Variation (%)	$\binom{-15}{+10}$	A	88.6	71.8	67.2	53.1	56.6
		B	99.7	99.0	98.3	97.1	93.4
	$\binom{-25}{+15}$	A	80.9	68.5	51.6	28.3	13.3
		B	99.3	98.6	97.7	96.3	95.3
Balance (%)*	33	A	86.0	79.5	75.2	62.1	54.4
		B	99.3	99.2	98.6	97.1	96.6
		A	85.5	77.3	73.6	57.1	48.4
		B	97.7	97.3	95.3	92.4	91.6
One feeder outage		A	81.7	72.9	66.2	62.6	51.4
		B	95.3	94.6	94.4	93.8	94.2

Table 4.4 HIF line identification in 13-node feeder in different conditions

Load		plan	400 Ω	800 Ω	1.2 kΩ	5 kΩ	15 kΩ
Base load		A	96.9	91.4	77.4	64.7	64.4
		B	96.4	94.8	95.4	95.3	95.9
Variation (%)	$\binom{-15}{+10}$	A	95.4	94.9	66.1	58.4	56.6
		B	94.9	94.3	94.3	94.3	93.4
	$\binom{-25}{+15}$	A	91.7	86.1	49.2	33.9	21.5
		B	92.8	93.3	93.3	92.3	91.8
Balance (%)*	33	A	94.4	93.7	76.1	58.4	52.6
		B	92.8	93.3	93.3	92.3	91.8
	67	A	94.4	93.3	71.0	55.2	49.1
		B	95.2	94.9	94.3	93.7	94.1
One feeder outage		A	88.8	91.4	72.4	58.1	52.7
		B	93.7	93.8	91.2	92.3	89.0

Table 4.5 HIF line identification in 123-node feeder in different conditions

*Blance: 33% of the single-phase loads are balanced to see the influence of load-balancing on the proposed HIF detection method

The two location approaches proposed in section 4, which are with and without intrinsic error correction, are evaluated on all aforementioned cases; i.e., 1000 runs are performed with intrinsic error correction and another 1000 runs are performed without intrinsic error correction for each case (marked in tables 4 and 5, as Plan A: without intrinsic error correction, and Plan B: with intrinsic error correction). The results generally demonstrate that the proposed approach performs reliably if the DS-SE model is calibrated by subtracting the intrinsic error of different bias estimates at their nominal value (i.e. at the nominal loads and generation). The results in tables 4 and 5 show that when the intrinsic error estimation has been saved according to the proposed procedure, the results of the location algorithm are fairly reliable compared to the reported literature average accuracy of 97.1%, while unlike other methods in the literature, the proposed method does not require separate measurements with high sampling rates. However, if the intrinsic error is not saved, the detection is less reliable. It is also observed that the intrinsic

error correction gives considerably accurate HIF line estimations in 123-bus system and has slightly more error in 13-bus system. The results of normal SE (without intrinsic error correction), on the contrary performs better in 13-bus than 123-bus system. This is mainly due to the large dimension of the suspected parameters ψ of (29) in 123-bus system. It is worth highlighting again that the intrinsic errors of bias estimates is saved only one time under the nominal loads at all buses without any HIF with only measurement errors (which are filtered by the estimator).

4.5 HIF distance estimation from the nodes

After determining the HIF line, the estimated values of biases can be used to find the location of HIF. Distribution systems are typically characterized by short lines, therefore identifying the faulty line is usually sufficient for DS operators in most of the cases, and an inspection will be conducted on the detected line. However, in case of long, or more importantly, underground lines, the accurate estimation of the HIF location may save a lot of time and costs for inspection. The proposed estimation approach to HIF location also provides an estimation of the HIF distance from the end node. In this subsection, results of the HIF distance estimation from the end node is presented. To this end, 99 HIFs are considered on uniformly increasing distances from end node of line 684-652 of 13-bus system as well as the line 57-60 of 123-bus system. The location procedure is performed 100 times for each of the 99 HIF cases, then the mean value and variance of estimation (of 100 runs at each distance) is plotted for each system in Fig. 3 (a) and (b). The HIF distance estimation on the other lines also exhibit the same behavior as those in Fig. 3, with least error in the middle of line and most error on two sides, because the defined parameter a in (1.c) is either zero or infinite on the two sides of the line.

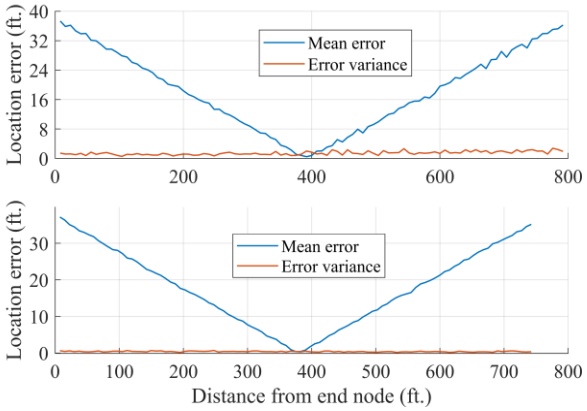

Figure 4.1 HIF distance estimation error in lines (a) 684-652 in 13-bus system with 800 ft. length and (b) 57-60 in 123-bus system with 750 ft. length

4.6 Individual HIF simulation

Subsections 4.2 shows the reliable performance of the detection for HIF existence, and subsection 4.3 shows the overall performance of the HIF line identification statistically, where it was observed the proposed approach is quite reliable. Now we take a look in the details of the results that was reported statistically in previous sections. We assume the HIF on the middle of the individual lines, and then we examine different impedance values for the HIF to evaluate the detection performance. The mathematical expectations are reported in this subsection by setting the measurement noise equal to zero deterministically.

- HIF location: line 632-633 phase *a*

HIF detection	plan	400 Ω	800 Ω	1.2 kΩ	5 kΩ	15 kΩ
	A*	632a-633a	632a-633a	632a-671a	632a-671a	671c-680c
	B**	632a-633a	632a-633a	632a-633a	632a-633a	632a-633a

Table 4.6 Individual HIF line identification results: HIF on line 632-633 phase *a*

- HIF location: line 671-675 phase *b*

HIF detection	plan	400 Ω	800 Ω	1.2 kΩ	5 kΩ	15 kΩ
	A*	671b-675b	671b-675b	671b-680b	671b-680b	671c-680c
	B**	671b-675b	671b-675b	671b-675b	671b-675b	671b-675b

Table 4.7 Individual HIF line identification results: HIF on line 671-675 phase *b*

- HIF location: line 671-680 phase *b*

HIF detection	plan	400 Ω	800 Ω	1.2 kΩ	5 kΩ	15 kΩ
	A*	671b-680b	671b-680b	671b-680b	671b-680b	675c-680c
	B**	671b-680b	671b-680b	671b-680b	671b-680b	671b-680b

Table 4.8 Individual HIF line identification results: HIF on line 671-680 phase *b*

- HIF location: line 632-633 phase *c*

HIF detection	plan	400 Ω	800 Ω	1.2 kΩ	5 kΩ	15 kΩ
	A*	632c-633c	632a-633a	632c-633c	632c-633c	632c-633c
	B**	632c-633c	632c-633c	632c-633c	632c-633c	632c-633c

Table 4.9 Individual HIF line identification results: HIF on line 632-633 phase *c*

- HIF location: line 632-645 phase *c*

HIF detection	plan	400 Ω	800 Ω	1.2 kΩ	5 kΩ	15 kΩ
	A*	632c-645c	632c-645c	632c-645c	632c-645c	632c-645c
	B**	632c-645c	632c-645c	632c-645c	632c-645c	632c-645c

Table 4.10 Individual HIF line identification results: HIF on line 632-645 phase *c*

- HIF location: line 632-671 phase *c*

HIF detection	plan	400 Ω	800 Ω	1.2 kΩ	5 kΩ	15 kΩ
	A*	632c-671c	632c-671c	632c-671c	632c-671c	632c-680c
	B**	632c-671c	632c-671c	632c-671c	632c-671c	632c-671c

Table 4.11 Individual HIF line identification results: HIF on line 632-671 phase *c*

4.7 Determining the HIF location performance on different nodes of the system

It was observed from the results of previous subsection that the performance of the proposed algorithm varies for HIFs on different feeders. Therefore, we define a performance criterion to evaluate the certainty of the located HIFs. Following the same logic of the previous subsection, we define three conditions: i) the HIF is located correctly (green), ii) the HIF is located at a neighboring feeder (yellow) and iii) HIF is located completely wrong (red). We give a score of +1 to the correctly located HIF, 0 to the HIFs located at neighboring feeders and -1 to the wrong location results. Then we evaluate different HIFs in the range of 400 Ω to 15 $k\Omega$, from which we obtain a performance criterion for each possible HIF on different nodes of the system. Mathematically speaking, we define a performance criterion η at each line, which is obtained from the following procedure. First, the HIF values are selected to be increasing from 400 Ω to 15 $k\Omega$. Because the power of the HIF is used in the algorithm, which is related to impedance inversely, the steps are chosen to be increasing via the reciprocal function, i.e. HIFs are selected on the points shown in the figure 4.2.

In other words, we apply the HIFs as shown in the figure 4.2 to each feeder of the systems individually, which include 25 different HIF values. Then we associate +1 score to the location

performance if it locates the HIF correctly, 0 score if it locates a neighboring feeder to the actual HIF, and -1 score if it locates the HIF wrong. Finally, the score of the HIF location algorithm at each feeder is the sum of the 25 different HIF values, according to the equations (4.2.a) and (4.2.b).

$$\eta = \sum_{i=1}^{25} s(HIF_i) \tag{4.2.a}$$

$$s(HIF_i) = \begin{cases} +1 & Location\ is\ correct \\ 0 & Neighboring\ feeder \\ -1 & Location\ is\ wrong \end{cases} \tag{4.2.b}$$

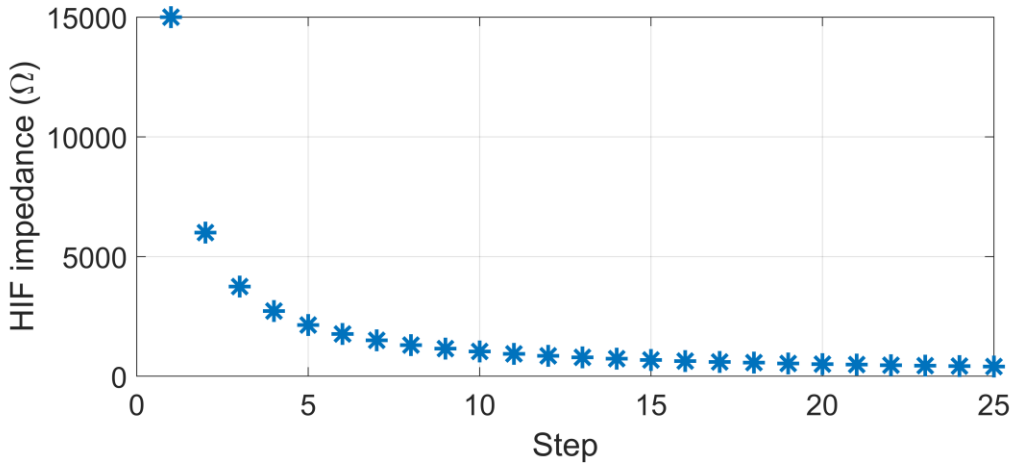

Figure 4.2 The steps of changing the HIF to evaluate the HIF location criteria of all feeders

The performance criteria η is plotted for the HIFs on different feeders of the 13-bus system in figure 4.3 as a heat-map where the criteria η is represented by the color of branches. Note that the two branches 632-645 and 684-652 are not considered as suspected nodes for having HIF, thus the performance criteria are not associated with these two branches. The performance criteria is +1 if it is able to locate all of the HIFs varying from 400 Ω to 15 $k\Omega$, and it is -1 if does not locate any of the HIFs in the specified range. After considering the set of suspected HIF branches as discussed, the defined performance criteria η is always positive in all of the branches of 13-node and 123-node feeders. Therefore, we mapped the "autumn" color map on η in range of zero to +1

to distinguish between different values of η. Similarly, 70 branches of the 123-node feeder are assumed as HIF-suspected feeders. The performance criteria of each of the 70 branches are plotted using the heat-map in the figure 4.4. Although the performance criteria has the range from -1 to +1, the colors are mapped on the range of η=0 to η=1 in order to distinguish between the η values. It is because after considering the suspected HIF branches as discussed, the performance criteria is always greater than 0 for all of the considered branches.

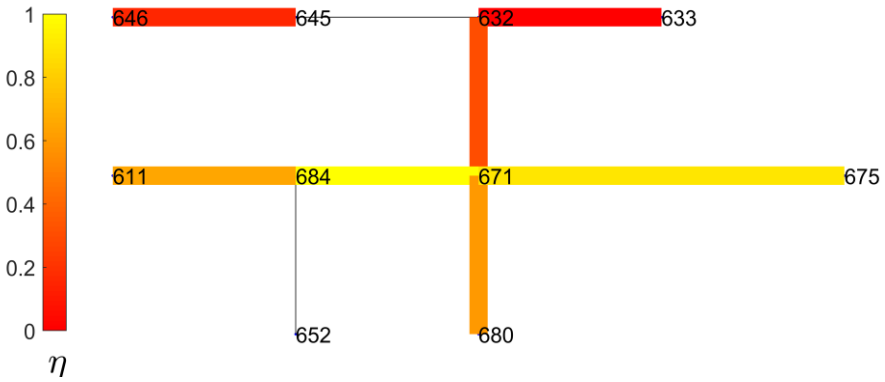

Figure 4.3 Performance criteria (4.2) for HIF line identification in 13-node feeder

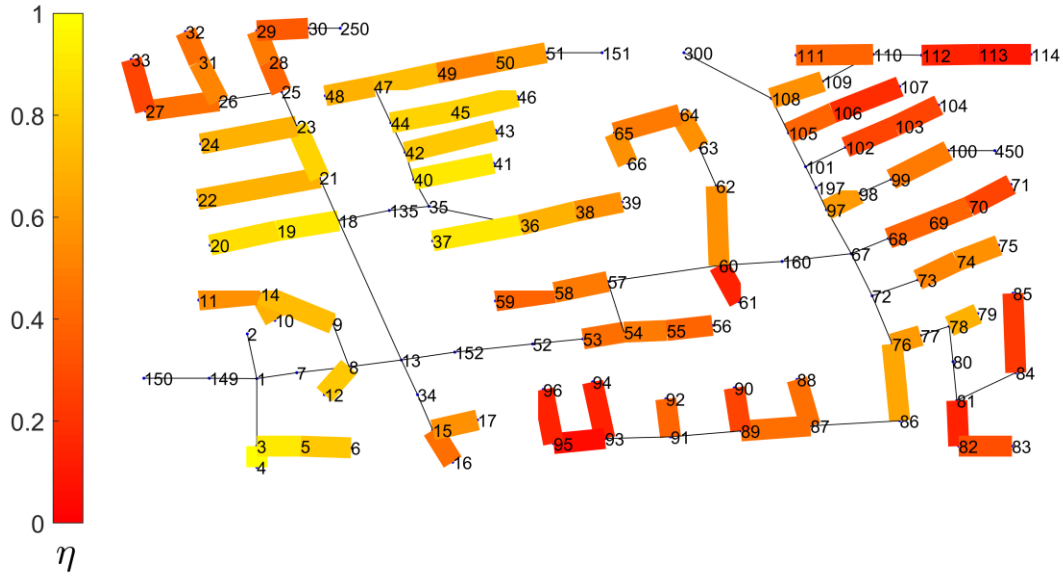

Figure 4.4 Performance criteria (4.2) for HIF line identification in 123-node feeder

4.8 Computational specification of the state estimation

The original state estimation, as discussed, is usually based on the WLS, to which the computational requirement of the proposed algorithm is compared, as reported in Table 4.12. The simulations are performed on a computer with a core-i5 CPU with 1.8 GHz frequency and 16 GB of installed memory (RAM) with a 64-bit windows operating system. Three estimators are considered to clarify the computational requirements of the proposed algorithm: i) WLS is used to estimate the original DS states, ii) Kalman filter is used to estimate the original DS states, and iii) bias filter is used to estimate the original states and the HIF parameters simultaneously. It can be seen in Table 4.12 that the most significant computational efforts are due to using the Kalman filter instead of the WLS; whereas adding the HIF parameters to the states does not increase the computations too much, considering the proposed HIF estimator is based on the bias filter, which is a variation of Kalman filter. Therefore, it can be concluded that not the augmentation of the HIF parameters, but rather the use of Kalman filter is the reason for the increased computational requirement. It can be also noticed that the computational requirement in the proposed estimator does not exceed 1.5 times that of the original WLS. Therefore, it can be concluded that computational requirement should not be an obstacle in front of applying the proposed method.

Estimator	WLS	Kalman filter	Proposed HIF estimator
13-bus	36 μsec	49 μsec	52 μsec
123-bus	4410 μsec	6280 μsec	6800 μsec

Table 4.12 Computational specification of the proposed HIF estimation method compared with WLS

4.9 Summary

Different case studies are simulated on the IEEE 13-node and 123-node feeder systems, to evaluate the performance of the proposed algorithm. In general, the detection performance of the proposed algorithm is proved to be very reliable, as evident from the literature. The location performance of the algorithm is, however, more complex. If DS-SE is augmented with all possible HIF parameters from all of the system branches, then the location performance would not be reliable. Therefore, it was suggested that only the more suspected lines are augmented for HIF location in the DS-SE algorithm. Accordingly, 7 and 70 branches were augmented in DS-SE algorithm in 13-node and 123-node feeder systems, respectively, for which the location performance is proved to be reliable. Besides, the proposed algorithm performs differently for the HIFs on different branches of the systems. Therefore, a location performance criterion is defined, which is evaluated for all of the considered branches of the two systems under study, which shows sufficiently reliable results for the location performance of the proposed algorithm.

Chapter 5: Conclusion

5.1 Summary

High-impedance fault possess a special position in the study and research on distribution systems, because they impose many negative effects on the operation of the system, yet the existing methods to deal with the HIF are far more expensive than the economical feasibility of the existing distribution systems. On the other hand, the negative effects of the HIF is not as severe as short-circuit faults, hence, the HIF remained as a less noticed area in the distribution system study and research. The existing HIF detection methods require equipment of the system with very high-resolution measurement devices up to MHz, however, modern distribution systems are moving towards being monitored using the SCADA measurements or Smart Meters, which have much less sampling rates around one sample per several minutes, or using PMU devices that have at most 60 samples per second. It is shown in different areas of the distribution system research that the existing monitoring infrastructure (based on SCADA, PMU, Smart meters or combination of them) are able to provide many various desired functionalities, such as distributed energy resources control, system model identification, energy theft detection, etc. In this regard, we proposed using the existing distribution system monitoring infrastructure to detect and locate the high-impedance fault. HIF is thus modeled as static impedance and augmented in DS-SE model. The proposed algorithm is absolutely compatible with all other functionalities of the existing DS monitoring infrastructure, hence, it imposes no additional cost other than software update costs as proposed in this thesis. The main limitation of the proposed method is the lower accuracy in case of the very high-impedance values of HIF, which can be alleviated using the more measurement devices.

5.2 Future work

The proposed idea, as shown in the simulation, is not able to identify and locate the HIFs from the entire system at once. It requires prior knowledge about the feeders, which can be obtained from the historical maintenance data as the best source. However, if such data are not available, the simulations and online measurement data can be insightful for the selection and exclusion of feeders from the system feeders. Therefore, evaluating the proposed algorithm on a real distribution system with available historical data would be significantly valuable. Especially, if the historical maintenance data are available, the economic benefits of the proposed algorithm can be evaluated in long-term operation of the distribution system. Hence the following works are suggested to be further studied:

- The actual data from distribution system is required for validating the proposed method.
- The proposed method is vulnerable to the errors in the system model parameters (network impedances), so its performance should be evaluated under actual model parameter errors.
- The distribution system state estimator generates some consistent erroneous estimates for some special nodes, which is referred to by Zhao and Mili as leverage points. Prior knowledge of these erroneous estimates can solve the problem of HIF estimation in those nodes.
- System-specific estimator design can indeed improve the performance of the state estimator and the HIF locator in turn; e.g. identifying the suspected HIF feeders, pre-calibrating the HIF parameters' estimates, weighting the measurements and state estimates by system-specific covariance matrix design, etc.

Bibliography

[1] A. Ghaderi, H. L. Ginn III, and H. A. Mohammadpour, "High impedance fault detection: A review," *Electr. Power Syst. Res.*, vol. 143, pp. 376–388, 2017.

[2] C. L. Benner and B. D. Russell, "Practical high-impedance fault detection on distribution feeders," *IEEE Trans. Ind. Appl.*, vol. 33, no. 3, pp. 635–640, 1997, doi: 10.1109/28.585852.

[3] Q. Cui, K. El-Arroudi, and Y. Weng, "A feature selection method for high impedance fault detection," *IEEE Trans. Power Deliv.*, vol. 34, no. 3, pp. 1203–1215, 2019.

[4] A. N. Milioudis, G. T. Andreou, and D. P. Labridis, "Detection and location of high impedance faults in multiconductor overhead distribution lines using power line communication devices," *IEEE Trans. Smart Grid*, vol. 6, no. 2, pp. 894–902, 2014.

[5] A. N. Milioudis, G. T. Andreou, and D. P. Labridis, "Enhanced protection scheme for smart grids using power line communications techniques—Part I: Detection of high impedance fault occurrence," *IEEE Trans. Smart Grid*, vol. 3, no. 4, pp. 1621–1630, 2012.

[6] A. N. Milioudis, G. T. Andreou, and D. P. Labridis, "Enhanced protection scheme for smart grids using power line communications techniques—Part II: Location of high impedance fault position," *IEEE Trans. Smart Grid*, vol. 3, no. 4, pp. 1631–1640, 2012.

[7] D. C. T. Wai and X. Yibin, "A novel technique for high impedance fault identification," *IEEE Trans. Power Deliv.*, vol. 13, no. 3, pp. 738–744, 1998.

[8] S. Gautam and S. M. Brahma, "Detection of high impedance fault in power distribution systems using mathematical morphology," *IEEE Trans. Power Syst.*, vol. 28, no. 2, pp. 1226–1234, 2012.

[9] W. C. Santos, F. V Lopes, N. S. D. Brito, and B. A. Souza, “High-impedance fault identification on distribution networks,” *IEEE Trans. Power Deliv.*, vol. 32, no. 1, pp. 23–32, 2016.

[10] A. Ghaderi, H. A. Mohammadpour, H. L. Ginn, and Y.-J. Shin, “High-impedance fault detection in the distribution network using the time-frequency-based algorithm,” *IEEE Trans. Power Deliv.*, vol. 30, no. 3, pp. 1260–1268, 2014.

[11] J. R. Macedo, J. W. Resende, C. A. Bissochi Jr, D. Carvalho, and F. C. Castro, “Proposition of an interharmonic-based methodology for high-impedance fault detection in distribution systems,” *IET Gener. Transm. Distrib.*, vol. 9, no. 16, pp. 2593–2601, 2015.

[12] É. M. Lima, C. M. dos Santos Junqueira, N. S. D. Brito, B. A. de Souza, R. de Almeida Coelho, and H. G. M. S. de Medeiros, “High impedance fault detection method based on the short-time Fourier transform,” *IET Gener. Transm. Distrib.*, vol. 12, no. 11, pp. 2577–2584, 2018.

[13] A. A. Girgis, W. Chang, and E. B. Makram, “Analysis of high-impedance fault generated signals using a Kalman filtering approach,” *IEEE Trans. Power Deliv.*, vol. 5, no. 4, pp. 1714–1724, 1990.

[14] X. Wang *et al.*, “High impedance fault detection method based on variational mode decomposition and Teager–Kaiser energy operators for distribution network,” *IEEE Trans. Smart Grid*, vol. 10, no. 6, pp. 6041–6054, 2019.

[15] M. Sarlak and S. M. Shahrtash, “High-impedance faulted branch identification using magnetic-field signature analysis,” *IEEE Trans. Power Deliv.*, vol. 28, no. 1, pp. 67–74, 2012.

[16] A. Orlandi, F. Rachidi, and M. Paolone, “Extension of the unmatched-media time reversal

method to locate soft faults in transmission lines," *IEEE Trans. Electromagn. Compat.*, vol. 60, no. 5, pp. 1539–1545, 2018.

[17] L. U. Iurinic, A. R. Herrera-Orozco, R. G. Ferraz, and A. S. Bretas, "Distribution systems high-impedance fault location: A parameter estimation approach," *IEEE Trans. Power Deliv.*, vol. 31, no. 4, pp. 1806–1814, 2015.

[18] F. Passerini and A. M. Tonello, "Smart grid monitoring using power line modems: Anomaly detection and localization," *IEEE Trans. Smart Grid*, vol. 10, no. 6, pp. 6178–6186, 2019.

[19] S. H. Mortazavi, M. H. Javidi, and E. Kamyab, "Robust Wide Area Fault Location Considering Network Parameters Error," *IEEE Trans. Power Deliv.*, vol. 34, no. 3, pp. 786–794, 2019.

[20] G. Morales-España, J. Mora-Flórez, and H. Vargas-Torres, "Elimination of multiple estimation for fault location in radial power systems by using fundamental single-end measurements," *IEEE Trans. power Deliv.*, vol. 24, no. 3, pp. 1382–1389, 2009.

[21] S. Chakraborty and S. Das, "Application of smart meters in high impedance fault detection on distribution systems," *IEEE Trans. Smart Grid*, vol. 10, no. 3, pp. 3465–3473, 2018.

[22] H. Matsuo, T. Fujishima, T. Yamashita, and K. Hatase, "Relation between leakage impedance and equivalent salt deposit density on an insulator under a saltwater spray," *IEEE Trans. Dielectr. Electr. Insul.*, vol. 6, no. 1, pp. 117–121, 1999.

[23] Y. Liu, B. X. Du, and M. Farzaneh, "Self-normalizing multivariate analysis of polymer insulator leakage current under severe fog conditions," *IEEE Trans. Power Deliv.*, vol. 32, no. 3, pp. 1279–1286, 2017.

[24] I. Ramirez, R. Hernandez, and G. Montoya, "Measurement of leakage current for monitoring the performance of outdoor insulators in polluted environments," *IEEE Electr.*

Insul. Mag., vol. 28, no. 4, pp. 29–34, 2012.

[25] R. Chakraborty, "Performance of silicone rubber insulators under thermal and electrical stress," *IEEE Trans. Ind. Appl.*, vol. 53, no. 3, pp. 2446–2454, 2017.

[26] H. H. Kordkheili, H. Abravesh, M. Tabasi, M. Dakhem, and M. M. Abravesh, "Determining the probability of flashover occurrence in composite insulators by using leakage current harmonic components," *IEEE Trans. Dielectr. Electr. Insul.*, vol. 17, no. 2, pp. 502–512, 2010.

[27] K. Dehghanpour, Z. Wang, J. Wang, Y. Yuan, and F. Bu, "A Survey on State Estimation Techniques and Challenges in Smart Distribution Systems," *IEEE Trans. Smart Grid*, vol. 10, no. 2, pp. 2312–2322, 2019, doi: 10.1109/TSG.2018.2870600.

[28] C. Gonzalez, J. Tant, J. G. Germain, T. De Rybel, and J. Driesen, "Directional, high-impedance fault detection in isolated neutral distribution grids," *IEEE Trans. Power Deliv.*, vol. 33, no. 5, pp. 2474–2483, 2018.

[29] S. H. Mortazavi, Z. Moravej, and S. M. Shahrtash, "A searching based method for locating high impedance arcing fault in distribution networks," *IEEE Trans. Power Deliv.*, vol. 34, no. 2, pp. 438–447, 2018.

[30] F. C. Schweppe and J. Wildes, "Power System Static-State Estimation, Part I: Exact Model," *IEEE Trans. Power Appar. Syst.*, vol. PAS-89, no. 1, pp. 120–125, 1970, doi: 10.1109/TPAS.1970.292678.

[31] M. E. Baran and A. W. Kelley, "A branch-current-based state estimation method for distribution systems," *IEEE Trans. Power Syst.*, vol. 10, no. 1, pp. 483–491, 1995, doi: 10.1109/59.373974.

[32] J. Song, E. Dall'Anese, A. Simonetto, and H. Zhu, "Dynamic Distribution State Estimation

Using Synchrophasor Data," *IEEE Trans. Smart Grid*, vol. 11, no. 1, pp. 821–831, 2020, doi: 10.1109/TSG.2019.2943540.

[33] R. A. Jabr and B. C. Pal, "Iteratively re-weighted least absolute value method for state estimation," *IEE Proc. - Gener. Transm. Distrib.*, vol. 150, no. 4, pp. 385–391, 2003, doi: 10.1049/ip-gtd:20030462.

[34] Y. Chakhchoukh, H. Lei, and B. K. Johnson, "Diagnosis of Outliers and Cyber Attacks in Dynamic PMU-Based Power State Estimation," *IEEE Trans. Power Syst.*, vol. 35, no. 2, pp. 1188–1197, 2020, doi: 10.1109/TPWRS.2019.2939192.

[35] J. Zhao and L. Mili, "A Framework for Robust Hybrid State Estimation With Unknown Measurement Noise Statistics," *IEEE Trans. Ind. Informatics*, vol. 14, no. 5, pp. 1866–1875, 2018, doi: 10.1109/TII.2017.2764800.

[36] E. Handschin, F. C. Schweppe, J. Kohlas, and A. Fiechter, "Bad data analysis for power system state estimation," *IEEE Trans. Power Appar. Syst.*, vol. 94, no. 2, pp. 329–337, 1975.

[37] R. Singh, B. C. Pal, and R. A. Jabr, "Choice of estimator for distribution system state estimation," *IET Gener. Transm. Distrib.*, vol. 3, no. 7, pp. 666–678, 2009, doi: 10.1049/iet-gtd.2008.0485.

[38] Y. Chakhchoukh and H. Ishii, "Enhancing Robustness to Cyber-Attacks in Power Systems Through Multiple Least Trimmed Squares State Estimations," *IEEE Trans. Power Syst.*, vol. 31, no. 6, pp. 4395–4405, 2016, doi: 10.1109/TPWRS.2015.2503736.

[39] A. Tabakhpour and M. Abdelaziz, "Enhanced Bad Data Identification in Distribution System State Estimation," in *2018 IEEE Canadian Conference on Electrical & Computer Engineering (CCECE)*, 2018, pp. 1–5, doi: 10.1109/CCECE.2018.8447843.

[40] Y. Zhang and J. Wang, "Towards Highly Efficient State Estimation With Nonlinear Measurements in Distribution Systems," *IEEE Trans. Power Syst.*, vol. 35, no. 3, pp. 2471–2474, 2020, doi: 10.1109/TPWRS.2020.2967173.

[41] D. A. Haughton and G. T. Heydt, "A Linear State Estimation Formulation for Smart Distribution Systems," *IEEE Trans. Power Syst.*, vol. 28, no. 2, pp. 1187–1195, 2013, doi: 10.1109/TPWRS.2012.2212921.

[42] A. Abur, "A bad data identification method for linear programming state estimation," *IEEE Trans. Power Syst.*, vol. 5, no. 3, pp. 894–901, 1990, doi: 10.1109/59.65919.

[43] C. Xu and A. Abur, "A Massively Parallel Framework for Very Large Scale Linear State Estimation," *IEEE Trans. Power Syst.*, vol. 33, no. 4, pp. 4407–4413, 2018, doi: 10.1109/TPWRS.2017.2788360.

[44] Y. Lin and A. Abur, "A Highly Efficient Bad Data Identification Approach for Very Large Scale Power Systems," *IEEE Trans. Power Syst.*, vol. 33, no. 6, pp. 5979–5989, 2018, doi: 10.1109/TPWRS.2018.2826980.

[45] H. Karimipour and V. Dinavahi, "Parallel relaxation-based joint dynamic state estimation of large-scale power systems," *IET Gener. Transm. Distrib.*, vol. 10, no. 2, pp. 452–459, 2016, doi: 10.1049/iet-gtd.2015.0808.

[46] A. Abur and A. G. Exposito, *Power system state estimation: theory and implementation*. CRC press, 2004.

[47] M. Jin, J. Lavaei, and K. H. Johansson, "Power Grid AC-Based State Estimation: Vulnerability Analysis Against Cyber Attacks," *IEEE Trans. Automat. Contr.*, vol. 64, no. 5, pp. 1784–1799, 2019, doi: 10.1109/TAC.2018.2852774.

[48] K. C. Sou, H. Sandberg, and K. H. Johansson, "Data Attack Isolation in Power Networks

Using Secure Voltage Magnitude Measurements," *IEEE Trans. Smart Grid*, vol. 5, no. 1, pp. 14–28, 2014, doi: 10.1109/TSG.2013.2280658.

[49] M. G. Damavandi, V. Krishnamurthy, and J. R. Martí, "Robust Meter Placement for State Estimation in Active Distribution Systems," *IEEE Trans. Smart Grid*, vol. 6, no. 4, pp. 1972–1982, 2015, doi: 10.1109/TSG.2015.2394361.

[50] Y. Yao, X. Liu, and Z. Li, "Robust Measurement Placement for Distribution System State Estimation," *IEEE Trans. Sustain. Energy*, vol. 10, no. 1, pp. 364–374, 2019, doi: 10.1109/TSTE.2017.2775862.

[51] M. Gholami, A. Abbaspour, S. Fattaheian-Dehkordi, M. Lehtonen, M. Moeini-Aghtaie, and M. Fotuhi, "Optimal allocation of PMUs in active distribution network considering reliability of state estimation results," *IET Gener. Transm. Distrib.*, vol. 14, no. 18, pp. 3641–3651, 2020, doi: 10.1049/iet-gtd.2019.1946.

[52] K. Dehghanpour, Y. Yuan, Z. Wang, and F. Bu, "A Game-Theoretic Data-Driven Approach for Pseudo-Measurement Generation in Distribution System State Estimation," *IEEE Trans. Smart Grid*, vol. 10, no. 6, pp. 5942–5951, 2019, doi: 10.1109/TSG.2019.2893818.

[53] M. Pignati, L. Zanni, P. Romano, R. Cherkaoui, and M. Paolone, "Fault detection and faulted line identification in active distribution networks using synchrophasors-based real-time state estimation," *IEEE Trans. Power Deliv.*, vol. 32, no. 1, pp. 381–392, 2016.

[54] A. Gandluru, S. Poudel, and A. Dubey, "Joint Estimation of Operational Topology and Outages for Unbalanced Power Distribution Systems," *IEEE Trans. Power Syst.*, vol. 35, no. 1, pp. 605–617, 2019.

[55] S. A. Salinas and P. Li, "Privacy-preserving energy theft detection in microgrids: A state estimation approach," *IEEE Trans. Power Syst.*, vol. 31, no. 2, pp. 883–894, 2015.

[56] M. M. A. Abdelaziz and H. E. Farag, “An enhanced supervisory control for islanded microgrid systems,” *IEEE Trans. Smart Grid*, vol. 7, no. 4, pp. 1941–1943, 2016.

[57] Y. Lin and A. Abur, “Robust state estimation against measurement and network parameter errors,” *IEEE Trans. power Syst.*, vol. 33, no. 5, pp. 4751–4759, 2018.

[58] A. Nikander and P. Järventausta, “Identification of high-impedance earth faults in neutral isolated or compensated MV networks,” *IEEE Trans. Power Deliv.*, vol. 32, no. 3, pp. 1187–1195, 2017.

[59] I. D. Mayergoyz and W. Lawson, “Chapter 3 - AC Steady State,” I. D. Mayergoyz and W. B. T.-B. E. C. T. Lawson, Eds. San Diego: Academic Press, 1997, pp. 58–97.

[60] M. M. A. Abdelaziz, “New analysis and operational control algorithms for islanded microgrid systems,” 2014.

[61] B. Friedland, “Treatment of bias in recursive filtering,” *IEEE Trans. Automat. Contr.*, vol. 14, no. 4, pp. 359–367, 1969.

[62] A. Gómez-Expósito, C. Gómez-Quiles, and I. Džafić, “State estimation in two time scales for smart distribution systems,” *IEEE Trans. Smart Grid*, vol. 6, no. 1, pp. 421–430, 2014.

[63] A. Alimardani, F. Therrien, D. Atanackovic, J. Jatskevich, and E. Vaahedi, “Distribution system state estimation based on nonsynchronized smart meters,” *IEEE Trans. Smart Grid*, vol. 6, no. 6, pp. 2919–2928, 2015.

[64] C. Rudin *et al.*, “Analytics for power grid distribution reliability in New York City,” *Interfaces (Providence).*, vol. 44, no. 4, pp. 364–383, 2014.

[65] D. T. Radmer, P. A. Kuntz, R. D. Christie, S. S. Venkata, and R. H. Fletcher, “Predicting vegetation-related failure rates for overhead distribution feeders,” *IEEE Trans. Power Deliv.*, vol. 17, no. 4, pp. 1170–1175, 2002.

[66] P. Gross *et al.*, "Predicting electricity distribution feeder failures using machine learning susceptibility analysis," in *AAAI*, 2006, pp. 1705–1711.

[67] J. Zhao and L. Mili, "Vulnerability of the largest normalized residual statistical test to leverage points," *IEEE Trans. Power Syst.*, vol. 33, no. 4, pp. 4643–4646, 2018.

[68] T. Kim and S. J. Wright, "PMU placement for line outage identification via multinomial logistic regression," *IEEE Trans. Smart Grid*, vol. 9, no. 1, pp. 122–131, 2016.

[69] M. Esmaili, K. Gharani, and H. A. Shayanfar, "Redundant observability PMU placement in the presence of flow measurements considering contingencies," *IEEE Trans. Power Syst.*, vol. 28, no. 4, pp. 3765–3773, 2013.

[70] M. Asprou, E. Kyriakides, and M. Albu, "The effect of variable weights in a WLS state estimator considering instrument transformer uncertainties," *IEEE Trans. Instrum. Meas.*, vol. 63, no. 6, pp. 1484–1495, 2013.

[71] R. Isermann and M. Münchhof, *Identification of dynamic systems: an introduction with applications*. Springer Science & Business Media, 2010.

[72] "IEEE Standard for Synchrophasor Measurements for Power Systems," *IEEE Std C37.118.1-2011 (Revision of IEEE Std C37.118-2005)*. pp. 1–61, 2011, doi: 10.1109/IEEESTD.2011.6111219.